Accepted manuscript. Published in Journal of the Mechanics and Physics of Solids (2018). Version of record: https://doi.org/10.1016/j.jmps.2018.02.009.
© 2018. This manuscript version is made available under the CC-BY-NC-ND 4.0 license https://creativecommons.org/licenses/by-nc-nd/4.0/

Mechanics of adsorption-deformation coupling in porous media

Yida Zhang[1]

ABSTRACT

This work extends Coussy's macroscale theory for porous materials interacting with adsorptive fluid mixtures. The solid-fluid interface is treated as an independent phase that has its own mass, momentum and energy balance laws. As a result, a surface strain energy term shows up in the free energy balance equation of the solid phase, which further introduces the so-called adsorption stress in the constitutive equations of the porous skeleton. This establishes a fundamental link between the adsorption characteristics of the solid-fluid interface and the mechanical response of the porous media. The thermodynamic framework is quite general in that it recovers the coupled conduction laws, Gibbs isotherm and the Shuttleworth's equation for surface stress, and imposes no constraints on the magnitude of deformation and the functional form of the adsorption isotherms. A rich variety of coupling between adsorption and deformation is recovered as a result of combining different poroelastic models (isotropic vs. anisotropic, linear vs. nonlinear) and adsorption models (unary vs. mixture adsorption, uncoupled vs. stretch-dependent adsorption). These predictions are discussed against the backdrop of recent experimental data on coal subjected to CO_2 and CO_2-CH_4 injections, showing the capability and versatility of the theory in capturing adsorption-induced swelling behaviours of porous materials.

Keywords: Poromechanics; adsorption; finite strain; interface; swelling; coal.

1 BACKGROUND

Classical poromechanics concerns the response of fluid-saturated porous media subjected to external forces and pore pressure changes. In the last decades, the original linear theory has been generalized for finite deformations (Biot, 1977; Gajo, 2010; Nedjar, 2013; Selvadurai and Suvorov, 2016), reformulated for analytical advantages (Anand, 2015; Rice and Cleary, 1976; Rudnicki, 1986), and included material inelasticity (Anand, 2017; Armero, 1999; Karrech et al., 2012). These theories belong to the so-called purely macroscale approaches in the sense that the constitutive responses are either defined a priori (e.g. Nur and Byerlee (1971)) or derived from a macroscopic Ψ-potential of the overall representative elementary volume (REV) (e.g. Biot (1972), Coussy (2004)). Another approach follows the theory of mixtures (Atkin and Craine, 1976; Truesdell, 1962) in which the mixture is represented by spatially superposed interacting continua with the kinematics of each constituent described by Eulerian quantities. When specialized for porous media, one of the constituents is assigned as the solid phase and volume fractions are introduced to highlight the immiscibility between solid and fluid (Bedford and Drumheller, 1983; Bowen, 1980; Pence, 2012). The constitutive relations of each constituent are derived from separate energy potentials and the macroscopic behaviour of the mixture is a result of averaging. Such formulation to certain extent reflects the microscale features of the porous media through the so-called *closure conditions* that govern the evolution of volume fraction of each constituent (de Boer, 1996). Candidates serving such condition include separate constitutive laws for volume fractions (Kenyon, 1976), balance of equilibrated forces or balance of porosity (Nunziato and Cowin, 1979; Wilmanski, 1998), internal constraints enforced in the entropy inequality (de Boer, 1996; Svendsen and Hutter, 1995), and dynamic compatibility conditions on the

[1] University of Colorado Boulder, Department of Civil, Environmental and Architectural Engineering, Boulder, CO, USA

interfaces (Wei and Muraleetharan, 2002). Readers shall refer to de Boer (2006) for a comprehensive survey. Mixture-based theories have been recently adapted for swelling and structural degradation of finitely strained polymers (Baek and Pence, 2009; Duda et al., 2010). In general, approaches based on mixture theory are more rigorous and generic as they are derived from the fundamental balance laws of the system and can account for arbitrary number of constituents that could be miscible or immiscible and chemically inert or active. On the other hand, purely macroscale theories enjoy their straightforwardness and permit analytical solutions for important initial-boundary value problems related to engineering practices (e.g. Abousleiman and Cui (1998); Cheng (2016)). Coussy (2004; 1998a) has shown that Biot's theory can be derived by reformulating the balance equations from mixture theories in terms of macroscopically measurable quantities, thus elucidating a profound connection between the two approaches. Specifically, the Lagrangian Clausius-Duhem inequality of the fluid-saturated porous media has been derived from the Eulerian balance equations of mass, momentum and energy of individual components. This inequality implies the existence of a single free energy potential that embodies the constitutive relations between the strain, fluid mass variation and temperature of the REV, which further leads to the usual thermoporoelasticity upon linearization. Such procedure has provided a thermodynamic foundation for Biot's theory and opened new avenues for the macroscale theories to benefit from the generality of mixture theories, i.e. to account for variably saturated conditions (Coussy, 2007), phase transitions (Coussy et al., 1998b) and chemical reactions (Coussy, 2010). The present study aims at continuing this line of development and formulating a purely macroscale theory for porous media immersed in adsorptive fluid mixtures.

The coupling between the adsorption/desorption of fluid molecules on pore surfaces and the mechanical response of porous solid has attracted growing research interest from physical chemistry, geological science, and energy industry (Cui and Bustin, 2005; Espinoza et al., 2014; Vandamme et al., 2010). One of the main drives is to understand and predict the swelling of coals during CO_2 sequestration, a process that changes the permeability of coal seams and impacts the efficiency of methane recovery. It has been observed that injecting CO_2 in methane-saturated coal seams can initially decrease the injectivity, followed by a permeability rebound as gas pressure increases (Palmer and Mansoori, 1996; Robertson, 2005). Experiments on unconfined coal samples have shown that the total strain increase monotonically with CO_2 pressure at low pressures (0~20 MPa) (George and Barakat, 2001; Levine, 1996), then may turn to contraction as the gas pressure keep increasing (> 20 MPa) (Hol and Spiers, 2012). Similar coupling effect has been observed on other porous materials, e.g. Whaporous glass (Scherer, 1986), metal-organic frameworks (Neimark et al., 2011), porous silicon (Dolino et al., 1996), silica aerogel (Reichenauer and Scherer, 2001) and zeolite (Sorenson et al., 2008). Early empirical models adopt Langmuir-like equations to link the swelling strain to gas pressure (Chikatamarla et al., 2004; Levine, 1996; Palmer and Mansoori, 1996). They cannot predict the contraction of coal at high pressures and are disconnected with fundamental physical principles. Recent thermodynamic models emphasize the role of surface energy in adsorption/desorption induced swelling/ shrinkage of porous materials. They conceptualize surface tension of the solid-fluid interface as a "prestress" on the solid skeleton which causes some initial elastic strain even under apparently stress-free condition. Adsorption decreases the surface tension and such prestress, consequently releasing part of the elastic strain and appearing as swelling of the porous solid. These models can quantitatively capture the evolution of strain and permeability during CO_2 pressurization (Li and Feng, 2016; Pan and Connell, 2007; Vandamme et al., 2010). The existence of a swelling-contraction transition point and the anisotropic swelling behaviour of coal specimens have also been predicted (Espinoza et al., 2013).

Despite their successes, the thermodynamic foundations of porous continua in adsorptive fluids have not been rigorously derived as done for the poromechanics theory by Coussy et al. (1998a), and no reference has been made to the balance laws established in mixture theories. This has created certain ambiguities. For example, many approaches rely on the following additive form of the free energy f_s (Li and Feng, 2016; Vandamme et al., 2010):

$$f_s(\varepsilon, \mathbf{e}, \phi) = \Psi_s(\varepsilon, \mathbf{e}, \phi) + u_{surf}(\varepsilon, \mathbf{e}, \phi) \tag{1}$$

where Ψ_s the Helmholtz free energy of the skeleton; u_{surf} is a new term account for energy storage in surface; ε the volumetric strain; $\mathbf{e}$ the strain deviator; ϕ the porosity. A consequence of such decomposition is that, an extra stress term called the *adsorption stress* σ_a appears as part of the work-conjugated stress of elastic strain (Coussy, 2010; Vandamme et al., 2010), through which the aforementioned prestress effect can be taken into account. However, the thermodynamic origin u_{surf} and its proper independent variables are not clear. According to Eq. (1), u_{surf} depends only on the kinematics of the skeleton $(\varepsilon, \mathbf{e}, \phi)$, assuming such energy can only be altered by mechanically stretching the interface $du_{surf} = \sigma^s dA_s$ where $A_s = A_s(\varepsilon, \mathbf{e}, \phi)$ is specific surface area and σ^s is surface stress. Then σ^s is made to depend on the chemical potential μ_i^f of the adsorbates to model adsorption-induced swelling. A consistency question naturally follows: should u_{surf} also depends on the states of the saturating fluid, thus having μ_i^f enters the arguments of u_{surf}? A further question is, is the additive structure of the free energy Eq. (1) merely a constitutive hypothesis, or does it have its root in the balance laws of the mixture? To answer these questions, it is necessary to revisit the thermodynamics of macroscale poromechanics and explicitly acknowledge solid-fluid interface in the system of interest.

The purpose of study is therefore two-fold: 1) to derive the balance laws for saturated adsorptive porous media that has surface as the third phase, hoping to justify u_{surf} in Eq. (1) and clarify its independent variables; 2) to show the capability of this framework in modelling adsorption-induced swelling of porous materials against the backdrop of recent experimental results on CO_2 infiltrated coals. The paper is structured as follows: the mass, mole, momentum, and energy balance equations including the contributions from the surface phase are derived in sections 2. The coupled conduction laws derived from the Clausius-Duhem inequality are shortly discussed in section 3. The free energy balance equations for the three phases are exploited in section 4, leading to the state equations of the fluid mixture, the Gibbs isotherm and the Shuttleworth's equation for surface stress, and the constitutive equations of the solid. Specific theories are put forward to interpret the swelling-contraction behaviour of coal specimens during the injection of pure CO_2 and CO_2-CH_4 mixtures (section 5). The implications of stretch-dependent adsorption and finite deformation of porous skeleton are discussed in section 6.

2 BALANCE LAWS

2.1 Kinematics and notations

Consider a system depicted in Fig. 1. The solid skeleton is deformable and chemically inert (i.e. does not exchange mass with the surrounding). The motion of the solid is described via $\mathbf{x} = \mathbf{x}(\mathbf{X}, t)$ where $\mathbf{x}$ is the

spatial position and **X** is the position of the solid particle at time t=0. A line segment $d\mathbf{X}$ and a volume element $d\Omega_0$ in the reference configuration map to the current configuration $d\mathbf{x}$ and $d\Omega_t$ via:

$$d\mathbf{x} = \mathbf{F} \cdot d\mathbf{X} \text{ and } d\Omega_t = Jd\Omega_0 \tag{2}$$

where $\mathbf{F} = \nabla_X \mathbf{x}$ is the deformation gradient; $J = \det \mathbf{F}$ is the Jacobian. The Green-Lagrangian strain is defined by $\mathbf{E} = \left(\nabla_X \mathbf{u}^s + {}^T\nabla_X \mathbf{u}^s + {}^T\nabla_X \mathbf{u}^s \cdot \nabla_X \mathbf{u}^s\right)/2$ where $\mathbf{u}^s = \mathbf{x} - \mathbf{X}$ is the displacement vector and ∇_X denotes gradient with respect to material coordinate **X**. The Eulerian description of the solid kinematics involves the use of velocity $\mathbf{V}^s(\mathbf{x},t)$ and the rate of deformation $\mathbf{D} = \left(\nabla_x \mathbf{V}^s + {}^T\nabla_x \mathbf{V}^s\right)/2$ where ∇_x denotes gradient with respect to spatial coordinate **x**. **D** and **E** are related by $\mathbf{D} = {}^T\mathbf{F}^{-1} \cdot (d\mathbf{E}/dt) \cdot \mathbf{F}^{-1}$.

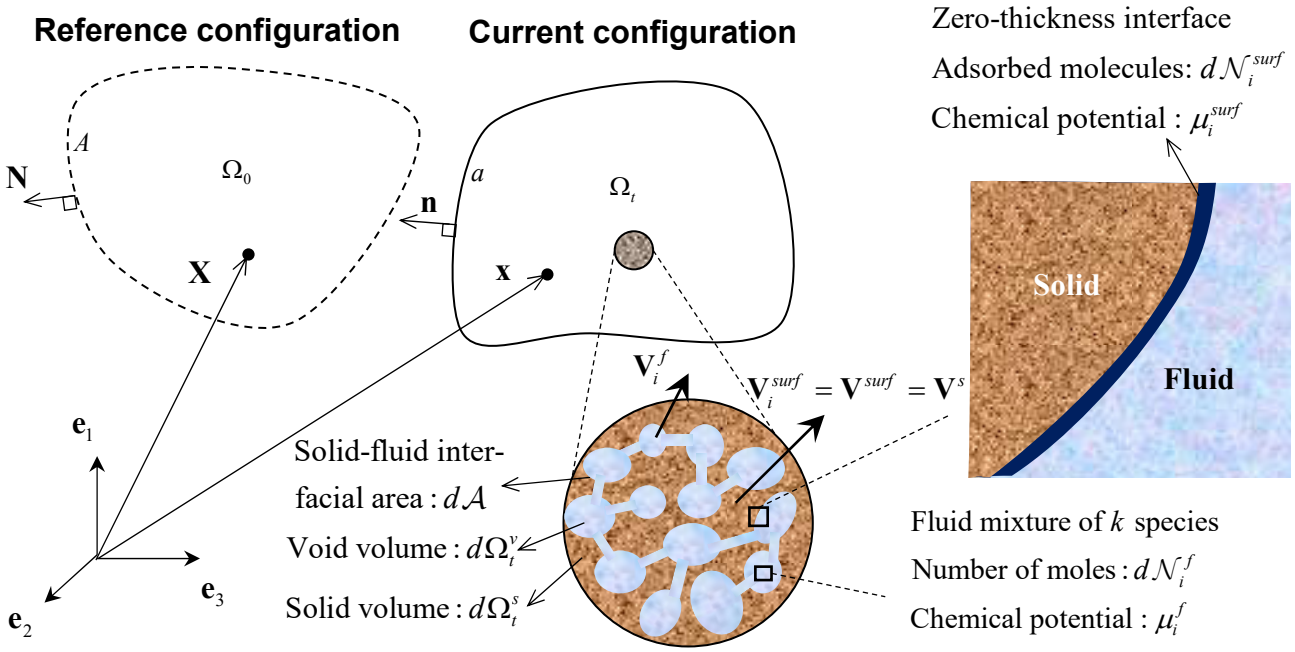

Fig.1: Schematics of a porous media immersed in adsorptive fluid mixture.

The void space $d\Omega_t^v$ in the in the representative volume $d\Omega_t$ is occupied by a mixture of k adsorptive fluid species. The Eulerian and Lagrangian porosity n and ϕ are defined as $d\Omega_t^v = nd\Omega_t = \phi d\Omega_0$. In between the solid and the fluid phases presents the surface phase (Fig. 1) which has zero thickness but possesses excess quantities such as mass, entropy and energy, just like an independent phase (DeHoff, 2006; Rice, 1978). Specific surface areas a_s and A_s are introduced to denote the amount of interface $d\mathcal{A}$ per unit current and reference volume, respectively:

$$d\mathcal{A} = a_s d\Omega_t = A_s d\Omega_0 \tag{3}$$

A species i can present in either fluid or surface phases due to adsorption/ desorption:

$$d\mathcal{N}_i = d\mathcal{N}_i^f + d\mathcal{N}_i^{surf} = n_i^f d\Omega_t + \Gamma_i^{surf} d\mathcal{A} \tag{4}$$

where $\mathcal{N}_i$, $\mathcal{N}_i^f$ and $\mathcal{N}_i^{surf}$ are the number of mole of species *i* in Ω_t overall, in the fluid phase, and in the solid phase respectively; Γ_i^{surf} is the surface excess concentration with a unit of mole/area; n_i^f is the number of mole in the fluid phase per unit current volume. The kinematics of species *i* can be described by separate velocities $\mathbf{V}_i^{surf}$ and $\mathbf{V}_i^f$ in the surface and fluid phases, respectively. The mass-averaged velocity of the bulk fluid is given by:

$$\mathbf{V}^f = \frac{1}{\rho_f}\sum \rho_i^f \mathbf{V}_i^f = \frac{1}{\rho_f n}\sum M_i n_i^f \mathbf{V}_i^f \tag{5}$$

where ρ_i^f is the mass of the species *i* per unit fluid volume; M_i is the molar mass; $\sum(\cdot)$ stands for $\sum_{i=1}^{k}(\cdot)$ if not specified otherwise. The particle derivative of a field with respect to phase α (= *s*, *f* or *surf*) is defined as:

$$\frac{d^\alpha}{dt}(\cdot) = \frac{\partial}{\partial t}(\cdot) + \mathbf{V}^\alpha \cdot \nabla_x(\cdot) \tag{6}$$

In this study, we assume that the surface moves together with the solid skeleton (i.e. $\mathbf{V}_i^{surf} = \mathbf{V}^{surf} = \mathbf{V}^s$). Thus $d^s(\cdot)/dt$ and $d^{surf}(\cdot)/dt$ are identical and only the former will be used for conciseness. Letters in the *MT extra* font denote extensive quantities (e.g. $\mathcal{E}$); Upper/ lower case Greek letters denote quantities in reference/ current configurations (e.g. *E* and *e*); letters with hat denote mass-related quantities (e.g. $\hat{e}_f$).

2.2 Mass and mole balance

Considering each phase as a subsystem, their mass balance can be expressed as:

$$\frac{d^s \rho_s (1-n)}{dt} + \rho_s (1-n)\nabla_x \cdot \mathbf{V}^s = 0 \tag{7}$$

$$\frac{d^s \rho_{surf} a_s}{dt} + \rho_{surf} a_s \nabla_x \cdot \mathbf{V}^s - \hat{r} = 0 \tag{8}$$

$$\frac{d^f \rho_f n}{dt} + \rho_f n \nabla_x \cdot \mathbf{V}^f + \hat{r} = 0 \tag{9}$$

where ρ_α is the intrinsic density of α phase (note ρ_{surf} has a unit of mass per unit area); $\hat{r}$ is the rate of adsorption by mass. In macroscopic theory, it is convenient to express the balance laws with respect to a fixed window that moves along with the solid skeleton. Eq. (9) may be rewritten as

$$\frac{d^s \rho_f n}{dt} + \rho_f n \nabla_x \cdot \mathbf{V}^s + \nabla_x \cdot \hat{\mathbf{w}} + \hat{r} = 0 \ \text{ or } \frac{\partial \rho_f \phi}{\partial t} + \nabla_X \cdot \hat{\mathbf{W}} + \hat{R} = 0 \tag{10}$$

where $\hat{\mathbf{w}} = \rho_f n\left(\mathbf{V}^f - \mathbf{V}^s\right)$ and $\hat{\mathbf{W}} = J\mathbf{F}^{-1} \cdot \hat{\mathbf{w}}$ are the Eulerian and Lagrangian relative flow vector, respectively; $\hat{R} = J\hat{r}$ is the Lagrangian rate of adsorption by mass.

Now focusing on individual species, their mole balance equations can be stated as:

$$\frac{d^s \Gamma_i^{surf} a_s}{dt} + \Gamma_i^{surf} a_s \nabla_x \cdot \mathbf{V}^s - r_i = 0 \tag{11}$$

$$\frac{d_i^f n_i^f}{dt} + n_i^f \nabla_x \cdot \mathbf{V}_i^f + r_i = 0 \tag{12}$$

where r_i is the rate of adsorption by mole. Eq. (12) can be also written with respect to a fixed solid window:

$$\frac{d^s n_i^f}{dt} + n_i^f \nabla_x \cdot \mathbf{V}^s + \nabla_x \cdot \mathbf{w}_i^f + r_i = 0 \text{ or } \frac{\partial N_i^f}{\partial t} + \nabla_X \cdot \mathbf{W}_i^f + R_i = 0 \tag{13}$$

where $\mathbf{w}_i^f = n_i^f \left(\mathbf{V}_i^f - \mathbf{V}^s \right)$ and $\mathbf{W}_i^f = J\mathbf{F}^{-1} \cdot \mathbf{w}_i^f$ are the relative flow vectors of component *i*; $R_i = Jr_i$ and $N_i^f = Jn_i^f$.

The smeared mass balance equations (8)-(10) must be identical with the summation of the mole balance (11)-(13) weighted by molar mass. This leads to several useful averaging relations:

$$\rho_{surf} = \sum M_i \Gamma_i^{surf} \; ; \; \hat{r} = \sum \hat{r}_i \; ; \; \hat{R} = \sum \hat{R}_i \tag{14}$$

$$\rho_f n = \sum M_i n_i^f \; ; \; \rho_f n \mathbf{V}^f = \sum M_i n_i^f \mathbf{V}_i^f \; ; \; \hat{\mathbf{w}} = \sum \hat{\mathbf{w}}_i^f \tag{15}$$

$$\rho_f \phi = \sum M_i N_i^f \; ; \; \hat{\mathbf{W}} = \sum \hat{\mathbf{W}}_i^f \tag{16}$$

where $\hat{r}_i = M_i r_i$, $\hat{R}_i = M_i R_i$, $\hat{\mathbf{w}}_i^f = M_i \mathbf{w}_i^f$ and $\hat{\mathbf{W}}_i^f = M_i \mathbf{W}_i^f$. The second equation in (15) is indeed the definition of mass-averaged fluid velocity (5).

For fluid mixtures, it is necessary to track the relative motion between component *i* and the bulk fluid. Introduce the diffusive mass flux vectors:

$$\hat{\mathbf{h}}_i^f = M_i n_i^f \left(\mathbf{V}_i^f - \mathbf{V}^f \right); \; \hat{\mathbf{H}}_i^f = J\mathbf{F}^{-1} \cdot \hat{\mathbf{h}}_i^f \tag{17}$$

One can verify $\sum \hat{\mathbf{h}}_i^f = 0$ and $\sum \hat{\mathbf{H}}_i^f = 0$ by substituting (17) into (5) and using the first equation of (15). The mismatch between $\mathbf{V}_i^f$ and $\mathbf{V}^f$ leads to the change of composition of the fluid mixture which is usually characterized by mass or mole fractions:

$$\hat{X}_i^f = \frac{M_i n_i^f}{\sum M_i n_i^f} = \frac{M_i n_i^f}{\rho_f n} = \frac{M_i N_i^f}{\sum M_i N_i^f} = \frac{M_i N_i^f}{\rho_f \phi} \; ; \; X_i^f = \frac{n_i^f}{\sum n_i^f} = \frac{N_i^f}{\sum N_i^f} \tag{18}$$

with $\sum \hat{X}_i^f = \sum X_i^f = 1$. Combining (17) and (18), the relative flow vectors can be rewritten as:

$$\hat{\mathbf{w}}_i^f = M_i n_i^f \left(\mathbf{V}_i^f - \mathbf{V}^s \right) = \hat{X}_i^f \rho_f n \left(\mathbf{V}^f - \mathbf{V}^s \right) + \hat{\mathbf{h}}_i^f = \hat{X}_i^f \hat{\mathbf{w}} + \hat{\mathbf{h}}_i^f \tag{19}$$

$$\hat{\mathbf{W}}_i^f = J\mathbf{F}^{-1} \cdot \hat{\mathbf{w}}_i^f = J\mathbf{F}^{-1} \cdot \left(\hat{X}_i^f \hat{\mathbf{w}} + \hat{\mathbf{h}}_i^f \right) = \hat{X}_i^f \hat{\mathbf{W}} + \hat{\mathbf{H}}_i^f \tag{20}$$

These relations are apparently consistent with Eqs. (15) and (16). The averaging relations (14)-(20) are important for algebraic simplifications in this study.

2.3 Momentum balance

The balance of linear momentum states

$$\frac{d^s}{dt}\int_{\Omega_t}\rho_s(1-n)\mathbf{V}^s d\Omega_t=\int_{\Omega_t}\rho_s(1-n)\mathbf{f}d\Omega_t+\int_{\partial\Omega_t}\mathbf{T}^s da+\int_{\Omega_t}\mathbf{P}^s d\Omega_t \tag{21}$$

$$\frac{d^s}{dt}\int_{\Omega_t}\rho_{surf}a_s\mathbf{V}^s d\Omega_t=\int_{\Omega_t}\rho_{surf}a_s\mathbf{f}d\Omega_t+\int_{\partial\Omega_t}\mathbf{T}^{surf}da+\int_{\Omega_t}\hat{r}\mathbf{V}^s d\Omega_t+\int_{\Omega_t}\mathbf{P}^{surf}d\Omega_t \tag{22}$$

$$\frac{d^f}{dt}\int_{\Omega_t}\rho_f n\mathbf{V}^f d\Omega_t=\int_{\Omega_t}\rho_f n\mathbf{f}d\Omega_t+\int_{\partial\Omega_t}\mathbf{T}^f da+\int_{\Omega_t}\left(-\hat{r}\right)\mathbf{V}^f d\Omega_t+\int_{\Omega_t}\mathbf{P}^f d\Omega_t \tag{23}$$

where $\mathbf{T}^\alpha=\boldsymbol{\sigma}^\alpha\cdot\mathbf{n}$ and $\boldsymbol{\sigma}^\alpha$ are the stress vector and tensor associated with phase α; $\mathbf{P}^\alpha$ represents the momentum exchange between phases and satisfies $\sum\mathbf{P}^\alpha=0$. Adsorption contributes to a momentum supply term $\hat{r}\mathbf{V}^s$ in Eq. (22) and correspondingly a momentum sink $-\hat{r}\hat{\mathbf{V}}^f$ in Eq. (23). Noticing Eqs. (7)-(9), the local form of Eqs. (21)-(23) are obtained as:

$$\nabla_x\cdot\boldsymbol{\sigma}^s+\rho_s(1-n)\left(\mathbf{f}-\boldsymbol{\gamma}^s\right)+\mathbf{P}^s=0 \tag{24}$$

$$\nabla_x\cdot\boldsymbol{\sigma}^{surf}+\rho_{surf}a_s\left(\mathbf{f}-\boldsymbol{\gamma}^s\right)+\mathbf{P}^{surf}=0 \tag{25}$$

$$\nabla_x\cdot\boldsymbol{\sigma}^f+\rho_f n\left(\mathbf{f}-\boldsymbol{\gamma}^f\right)+\mathbf{P}^f=0 \tag{26}$$

where $\boldsymbol{\gamma}^\alpha=d^\alpha\mathbf{V}^\alpha/dt$ is the acceleration vector of phase α. Summation of Eqs. (24)-(26) gives the overall balance of linear momentum:

$$\nabla_x\cdot\boldsymbol{\sigma}+\left[\rho_s(1-n)+\rho_{surf}a_s\right]\left(\mathbf{f}-\boldsymbol{\gamma}^s\right)+\rho_f n\left(\mathbf{f}-\boldsymbol{\gamma}^f\right)=0 \tag{27}$$

where $\boldsymbol{\sigma}=\boldsymbol{\sigma}^s+\boldsymbol{\sigma}^{surf}+\boldsymbol{\sigma}^f$ is the Cauchy stress tensor. The fluid partial stress is usually a spherical tensor $\boldsymbol{\sigma}^f=-np\mathbf{I}$ where p is fluid pressure (positive as compression) and $\mathbf{I}$ is the second-order identity tensor. Comparing to the momentum balance of non-reactive porous media (Coussy, 2004, Eq. 2.19), Eq. (27) has an additional term $\rho_{surf}a_s\left(\mathbf{f}-\boldsymbol{\gamma}^s\right)$ to account for the inertia and body force carried by the surface excess mass. Apparently, terms related with adsorption or momentum exchange do not appear in Eq. (27), confirming that mass or momentum cannot be created or diminished through internal processes.

2.4 The first law

The energy balance of each phase can be written as:

$$\frac{d^s}{dt}\int_{\Omega_t}\rho_s(1-n)\left(\hat{e}^s+\frac{1}{2}\mathbf{V}^{s2}\right)d\Omega_t=\int_{\Omega_t}\rho_s(1-n)\mathbf{f}\cdot\mathbf{V}^s d\Omega_t+\int_{\partial\Omega_t}\mathbf{T}^s\cdot\mathbf{V}^s da-\int_{\partial\Omega_t}\mathbf{q}^s\cdot\mathbf{n}da+\int_{\Omega_t}\mathbf{P}^s\cdot\mathbf{V}^s d\Omega_t+\int_{\Omega_t}\theta^s d\Omega_t \tag{28}$$

$$\frac{d^s}{dt}\int_{\Omega_t}\rho_{surf}a_s\left(\hat{e}^{surf}+\frac{1}{2}\mathbf{V}^{s2}\right)d\Omega_t=\int_{\Omega_t}\rho_{surf}a_s\mathbf{f}\cdot\mathbf{V}^s d\Omega_t+\int_{\partial\Omega_t}\mathbf{T}^{surf}\cdot\mathbf{V}^s da-\int_{\partial\Omega_t}\mathbf{q}^{surf}\cdot\mathbf{n}da+\int_{\Omega_t}\sum\hat{\mu}_i^{surf}\hat{r}_i d\Omega_t+\int_{\Omega_t}\frac{1}{2}\hat{r}\mathbf{V}^{s2}d\Omega_t+\int_{\Omega_t}\mathbf{P}^{surf}\cdot\mathbf{V}^s d\Omega_t+\int_{\Omega_t}\theta^{surf}d\Omega_t \tag{29}$$

$$\frac{d^f}{dt}\int_{\Omega_t}\rho_f n\left(\hat{e}^f+\frac{1}{2}\mathbf{V}^{f2}\right)d\Omega_t=\int_{\Omega_t}\rho_f n\mathbf{f}\cdot\mathbf{V}^f d\Omega_t+\int_{\partial\Omega_t}\mathbf{T}^f\cdot\mathbf{V}^f da-\int_{\partial\Omega_t}\mathbf{q}^f\cdot\mathbf{n}da+\int_{\Omega_t}\sum\hat{\mu}_i^f\left(-\hat{r}_i\right)d\Omega_t+\int_{\Omega_t}\frac{1}{2}\left(-\hat{r}\right)\mathbf{V}^{f2}d\Omega_t-\int_{\partial\Omega_t}\sum\hat{\mu}_i^f\hat{\mathbf{h}}_i^f\cdot\mathbf{n}da+\int_{\Omega_t}\mathbf{P}^f\cdot\mathbf{V}^f d\Omega_t+\int_{\Omega_t}\theta^f d\Omega_t \tag{30}$$

where $\hat{e}^\alpha$ is the mass-specific internal energy; θ^α represents the energy transfer to the α phase due to interaction with the other phases; $\mathbf{q}^\alpha$ is the surface heat flux vector; $\hat{\mu}_i^f$ and $\hat{\mu}_i^{surf}$ are the mass-specific chemical potentials of species *i* in the fluid and surface phases, respectively. On the RHS of Eqs. (29) and (30), the fourth term represents the change in internal energy due to species entering/ leaving the surface and fluid phases. The fifth term represents the gain/ loss of kinetic energy due to adsorption. The sixth term on the RHS of Eq. (30) represents the energy flux due to the movement of each species relative to the bulk fluid. The chemical potentials $\hat{\mu}_i^f$ and $\hat{\mu}_i^{surf}$ are introduced here as *primitive quantities* in the sense of Gurtin et al. (2010) to quantify the energy required to add one mole of component *i* in the corresponding phases. The axiom of energy balance of the mixture states that the energy transfer together θ^α with the work done by the momentum transfer $\mathbf{P}^\alpha\cdot\mathbf{V}^\alpha$ neither creates nor destroys the energy of the mixture (Pence, 2012):

$$\theta^s+\theta^{surf}+\theta^f+\mathbf{P}^s\cdot\mathbf{V}^s+\mathbf{P}^{surf}\cdot\mathbf{V}^s+\mathbf{P}^f\cdot\mathbf{V}^f=0 \tag{31}$$

The overall energy balance can be obtained by summing Eqs. (28), (29), (30) and considering (31):

$$\frac{d^s\left(\mathcal{E}_s+\mathcal{K}_s\right)}{dt}+\frac{d^s\left(\mathcal{E}_{surf}+\mathcal{K}_{surf}\right)}{dt}+\frac{d^f\left(\mathcal{E}_f+\mathcal{K}_f\right)}{dt}=\mathcal{P}_{\mathbf{f,T}}+\mathcal{Q}+\mathcal{T}+\mathcal{R} \tag{32}$$

where

$$\mathcal{E}_s=\int_{\Omega_t}\rho_s(1-n)\hat{e}^s d\Omega_t;\mathcal{E}_{surf}=\int_{\Omega_t}\rho_{surf}a_s\hat{e}^{surf}d\Omega_t;\mathcal{E}_f=\int_{\Omega_t}\rho_f n\hat{e}^f d\Omega_t \tag{33}$$

$$\mathcal{K}_s = \int_{\Omega_t} \frac{1}{2}\rho_s(1-n)\mathbf{V}^{s2}d\Omega_t ; \mathcal{K}_{surf} = \int_{\Omega_t} \frac{1}{2}\rho_{surf}a_s\mathbf{V}^{s2}d\Omega_t ; \mathcal{K}_f = \int_{\Omega_t} \frac{1}{2}\rho_f n\mathbf{V}^{f2}d\Omega_t \tag{34}$$

are the potential and kinetic energies for the solid, surface and fluid phases, respectively;

$$\mathcal{R} = -\int_{\Omega_t} \sum \left(\hat{\mu}_i^f - \hat{\mu}_i^{surf}\right)\hat{r}_i d\Omega_t - \int_{\Omega_t} \frac{1}{2}\hat{r}\left(\mathbf{V}^{f2} - \mathbf{V}^{s2}\right)d\Omega_t$$

is the rate of change of internal energy due to adsorption;

$$\mathcal{P}_{\mathbf{f},\mathbf{T}} = \int_{\Omega_t} \left[\rho_s(1-n)\mathbf{f}\cdot\mathbf{V}^s + \rho_{surf}a_s\mathbf{f}\cdot\mathbf{V}^s + \rho_f n\mathbf{f}\cdot\mathbf{V}^f\right]d\Omega_t + \int_{\partial\Omega_t}\left[\mathbf{T}^s\cdot\mathbf{V}^s + \mathbf{T}^s\cdot\mathbf{V}^s + \mathbf{T}^f\cdot\mathbf{V}^f\right]da \tag{35}$$

is the rate of external work;

$$\mathcal{Q} = -\int_{\partial\Omega_t}\mathbf{q}\cdot\mathbf{n}da = -\int_{\partial\Omega_t}\left(\mathbf{q}^s + \mathbf{q}^{surf} + \mathbf{q}^f\right)\cdot\mathbf{n}da \tag{36}$$

is the rate of heat exchange; and

$$\mathcal{T} = -\int_{\partial\Omega_t}\sum\hat{\mu}_i^f\hat{\mathbf{h}}_i^f\cdot\mathbf{n}da \tag{37}$$

is the energy flux due to species transport relative to the bulk fluid. The local form of Eq. (32) can be finally derived (see Appendix 1):

$$\frac{d^s e}{dt} + e\nabla\cdot\mathbf{V}^s = \boldsymbol{\sigma}:\mathbf{D} - \nabla_x\cdot\left(\hat{h}_f\hat{\mathbf{w}}\right) + \left(\mathbf{f}-\boldsymbol{\gamma}^f\right)\cdot\hat{\mathbf{w}} - \sum\left(\hat{\mu}_i^f - \hat{\mu}_i^{surf}\right)\hat{r}_i - \nabla_x\cdot\mathbf{q} - \sum\nabla_x\cdot\hat{\mu}_i^f\hat{\mathbf{h}}_i^f \tag{38}$$

or

$$\frac{\partial E}{\partial t} = \mathbf{S}:\frac{\partial\mathbf{E}}{\partial t} - \nabla_X\cdot\left(\hat{h}_f\hat{\mathbf{W}}\right) + \left(\mathbf{f}-\boldsymbol{\gamma}^f\right)\cdot\mathbf{F}\cdot\hat{\mathbf{W}} - \sum\left(\hat{\mu}_i^f - \hat{\mu}_i^{surf}\right)\hat{R}_i - \nabla_X\cdot\mathbf{Q} - \sum\nabla_X\cdot\hat{\mu}_i^f\hat{\mathbf{H}}_i^f \tag{39}$$

where

$$e = \rho_s(1-n)\hat{e}_s + \rho_{surf}a_s\hat{e}_{surf} + \rho_f n\hat{e}_f \text{ and } E = \rho_s(1-\phi)\hat{e}_s + \rho_{surf}A_s\hat{e}_{surf} + \rho_f\phi\hat{e}_f \tag{40}$$

e and E are the overall internal energy per unit current and reference volume, respectively; $\hat{h}_f$ is the mass-specific enthalpy of the fluid defined in Appendix 2; $\mathbf{S} = \mathbf{F}^{-1}\cdot J\boldsymbol{\sigma}\cdot(\mathbf{F}^T)^{-1}$ is the Second Piola-Kirchhoff stress; $\mathbf{Q} = J\mathbf{F}^{-1}\cdot\mathbf{q}$ is the Lagrangian heat flux vector. If the transport of individual species is prohibited and the fluid is non-adsorptive (i.e. $\hat{\mathbf{h}}_i^f = 0$, $\rho_{surf} = 0$ and $\hat{r}_i = 0$), Eq. (38) becomes identical to the energy balance for non-reactive porous media (Coussy, 2004, Eq. (3.19)). It is worth noting that, while internal processes do not affect the mass or momentum of the system, they can promote changes of the molecular configuration of the system towards more stable states. In this case, adsorption is driven by the difference between the chemical potentials (i.e. $\hat{r} > 0$ for $\hat{\mu}_i^f - \hat{\mu}_i^{surf} > 0$), leading to the release of the system's energy (i.e. exothermic).

2.5 The second law and the Clausius-Duhem inequality

The entropy inequality is enforced on the entire mixture rather than on the individual phases (de Boer, 2006):

$$\frac{d^s}{dt}\int_{\Omega_t}\rho_s(1-n)\hat{s}_s d\Omega_t+\frac{d^s}{dt}\int_{\Omega_t}\rho_{surf}a_s\hat{s}_{surf}d\Omega_t+\frac{d^f}{dt}\int_{\Omega_t}\rho_f n\hat{s}_f d\Omega_t\geq-\int_{\partial\Omega_t}\frac{\mathbf{q}^s\cdot\mathbf{n}}{T}da-\int_{\partial\Omega_t}\frac{\mathbf{q}^{surf}\cdot\mathbf{n}}{T}da-\int_{\partial\Omega_t}\frac{\mathbf{q}^f\cdot\mathbf{n}}{T}da \tag{41}$$

where $\hat{s}_\alpha$ is the mass-specific entropy of the α phase; T the absolute temperature. The local form of Eq. (41) is obtained as:

$$\frac{d^s s}{dt}+s\nabla_x\cdot\mathbf{V}^s\geq-\nabla_x\cdot\left(\hat{s}_f\hat{\mathbf{w}}+\frac{\mathbf{q}}{T}\right) \tag{42}$$

or

$$\frac{\partial S}{\partial t}\geq-\nabla_X\cdot\left(\hat{s}_f\hat{\mathbf{W}}+\frac{\mathbf{Q}}{T}\right) \tag{43}$$

where

$$s=\rho_s(1-n)\hat{s}_s+\rho_{surf}a_s\hat{s}_{surf}+\rho_f n\hat{s}_f \text{ and } S=Js=\rho_s(1-\phi)\hat{s}_s+\rho_{surf}A_s\hat{s}_{surf}+\rho_f\phi\hat{s}_f \tag{44}$$

are the overall entropy per unit current and reference volume, respectively. Denote Ψ as the total Helmholtz free energy per unit reference volume:

$$\Psi=E-TS \tag{45}$$

It can be similarly decomposed as:

$$\Psi=\rho_s\left(1-\phi\right)\hat{\psi}_s+\rho_{surf}A_s\hat{\psi}_{surf}+\rho_f\phi\hat{\psi}_f \tag{46}$$

The Clausius-Duhem inequality constraining the evolution of the system can be derived by substituting Eqs. (39), (45) and (46) into (43) (see Appendix 3):

$$\Phi_M+\Phi_H+\Phi_C+\Phi_T\geq0 \tag{47}$$

where:

$$\Phi_M=\mathbf{S}:\frac{\partial\mathbf{E}}{\partial t}+\hat{g}_f\frac{\partial\rho_f\phi}{\partial t}+\sum\hat{\mu}_i^f\left(\rho_f\phi\frac{\partial\hat{X}_i^f}{\partial t}+M_i\frac{\partial\Gamma_i^{surf}A_s}{\partial t}\right)-\sum\left(\hat{\mu}_i^f-\hat{\mu}_i^{surf}\right)\hat{R}_i-S\frac{\partial T}{\partial t}-\frac{\partial\Psi}{\partial t} \tag{48}$$

is the *material dissipation* due to deformation of the solid, surface and fluid phases, change in fluid composition, and temperature variations; $\hat{g}_f$ is the mass-specific Gibbs free energy of the fluid;

$$\Phi_H=-\left[\nabla_X\hat{g}_f-\left(\mathbf{f}-\boldsymbol{\gamma}^f\right)\cdot\mathbf{F}+\hat{s}_f\nabla_X T-\sum\hat{\mu}_i^f\nabla_X\hat{X}_i^f\right]\cdot\hat{\mathbf{W}} \tag{49}$$

is the *fluid transport dissipation* driven by relative flow $\hat{\mathbf{W}}$;

$$\Phi_C = -\sum \hat{\mathbf{H}}_i^f \cdot \nabla_X \hat{\mu}_i^f \tag{50}$$

is the *species diffusion dissipation* driven by the movement of species relative to the bulk fluid $\hat{\mathbf{H}}_i^f$;

$$\Phi_T = -\frac{\mathbf{Q}}{T} \cdot \nabla_X T \tag{51}$$

is the *thermal dissipation* due to heat flux **Q**. If the material evolution, fluid flow, species transport and heat conduction are regarded as relatively independent processes, (47) can be replaced by a stronger statement:

$$\Phi_M \geq 0, \Phi_H \geq 0, \Phi_T \geq 0, \Phi_C \geq 0 \tag{52}$$

The constitutive equations or conduction laws must satisfy the corresponding inequalities in (52). This study focuses on exploiting the material dissipation $\Phi_M > 0$. The implications of $\Phi_H \geq 0, \Phi_T \geq 0, \Phi_C \geq 0$ are only briefly discussed in the next section for completeness.

3 CONDUCTION LAWS

The last three inequalities in Eq. (52) can be re-expressed in Eulerian form:

$$\phi_H = -\frac{1}{\rho_f} \hat{\mathbf{w}} \cdot \left[\nabla_x p - \rho_f \left(\mathbf{f} - \boldsymbol{\gamma}^f \right) \right] \geq 0 \tag{53}$$

$$\phi_T = -\frac{\mathbf{q}}{T} \cdot \nabla_x T \geq 0 \tag{54}$$

$$\phi_C = -\sum \hat{\mathbf{h}}_i^f \cdot \nabla_x \hat{\mu}_i^f \geq 0 \tag{55}$$

Here the state equations in terms of $\hat{g}_f$ (Appendix 2, Eq. (129)) are invoked in deriving Eq. (53). The simplest conduction laws satisfying (53)-(54) have the linear form:

$$n\left(\mathbf{V}^f - \mathbf{V}^s\right) = -\mathbf{K} \cdot \left(\nabla_x p - \rho_f \mathbf{g}\right) \tag{56}$$

$$\mathbf{q} = -\boldsymbol{\kappa} \cdot \nabla_x T \tag{57}$$

$$\hat{\mathbf{h}}_i^f = -\sum_{j=1}^{k} \mathbf{L}^{ij} \cdot \nabla_x \hat{\mu}_j^f \tag{58}$$

where $\mathbf{K}$, $\boldsymbol{\kappa}$ and $\mathbf{L}^{ij}$ are permeability, thermal conductivity and mobility tensors which are symmetric and positive semi-definite. Eqs. (56)-(58) are the usual Darcy's, Fourier's and Fick's laws, respectively.

The three irreversible processes may be coupled, and thus a more general inequality should be stated:

$$\Phi_H + \Phi_C + \Phi_T \geq 0 \tag{59}$$

This leads to a single constraint for all the diffusion processes

$$\phi_H + \phi_T + \phi_C = -\frac{1}{\rho_f}\hat{\mathbf{w}}\cdot\left[\nabla_x p - \rho_f\left(\mathbf{f}-\boldsymbol{\gamma}^f\right)\right] - \frac{\mathbf{q}}{T}\cdot\nabla_x T - \sum \hat{\mathbf{h}}_i^f \cdot \nabla_x \hat{\mu}_i^f \geq 0 \tag{60}$$

Eq. (60) can be satisfied by the following generalized linear conduction law:

$$\begin{bmatrix} n\left(\mathbf{V}^f - \mathbf{V}^s\right) \\ \mathbf{q} \\ \hat{\mathbf{h}}_1^f \\ \hat{\mathbf{h}}_2^f \\ \vdots \\ \hat{\mathbf{h}}_k^f \end{bmatrix} = \overbrace{\begin{bmatrix} \Theta^{HH} & \Theta^{HT} & \Theta^{HC_1} & \dots & \Theta^{HC_k} \\ \Theta^{TH} & \Theta^{TT} & \Theta^{TC_1} & \dots & \Theta^{TC_k} \\ \Theta^{C_1H} & \Theta^{C_1T} & \Theta^{C_1C_1} & \dots & \Theta^{C_1C_k} \\ \vdots & \vdots & \vdots & \ddots & \vdots \\ \Theta^{C_kH} & \Theta^{C_kH} & \Theta^{C_kC_1} & \dots & \Theta^{C_kC_k} \end{bmatrix}}^{\boldsymbol{\Theta}^{\alpha\beta}} \begin{bmatrix} \nabla_x p - \rho_f\left(\mathbf{f}-\boldsymbol{\gamma}^f\right) \\ \nabla_x T \\ \nabla_x \hat{\mu}_1^f \\ \nabla_x \hat{\mu}_2^f \\ \vdots \\ \nabla_x \hat{\mu}_k^f \end{bmatrix} \tag{61}$$

where $\boldsymbol{\Theta}^{\alpha\beta}$ is positive-semidefinite $(k+2)\times(k+2)$ matrix with $\alpha,\beta = H,T,C_1,C_2...,C_k$. The coupling between the mechanically, thermally and chemically induced mass transports is supported by a large body of experimental evidence. For example, the flow of bulk fluid driven by concentration gradient is known as osmotic flow which plays a central role in porous membrane (Anderson and Malone, 1974; Wijmans and Baker, 1995) and swelling clays (Barbour and Fredlund, 1989; Bennethum et al., 1997; Huyghe and Janssen, 1997). Hydrothermal coupling is often attributed to the temperature-dependent density of the fluid and thus is also referred to as the buoyancy effect (Lapwood, 1948; Trevisan and Bejan, 1985). The dependency of the motion of individual species on pressure and temperature gradients is known as the Soret effect (Soret, 1880) and has been widely observed in experiments (Kolodner et al., 1988; Legros et al., 1985; Ning and Wiegand, 2006). Starting from fundamental conservation laws and a set of constitutive postulations, Hassanizadeh (1986) derived the generalized Darcy's and Fick's law that describe the mass transport subjected to combined pressure, temperature, and chemical potential gradients. Eq. (61) presents an alternative representation of these generalized laws that is derived from the coupled dissipation inequality (59).

4 CONSTITUTIVE LAWS

The material dissipation Φ_M can be further decomposed by substituting Eqs. (44) and (46) into (48) (see Appendix 3):

$$\Phi_M = \Phi_M^s + \Phi_M^{surf} + \Phi_M^f \geq 0 \tag{62}$$

where

$$\Phi_M^s = \mathbf{S}:\frac{\partial \mathbf{E}}{\partial t} + p\frac{\partial \phi}{\partial t} - S_s\frac{\partial T}{\partial t} - \left(\rho_{surf}\hat{\psi}_{surf} - \sum M_i \hat{\mu}_i^f \Gamma_i\right)\frac{\partial A_s}{\partial t} - \frac{\partial \rho_s\left(1-\phi\right)\hat{\psi}_s}{\partial t} + \sum\left(\hat{\mu}_i^{surf} - \hat{\mu}_i^f\right)\hat{R}_i \tag{63}$$

$$\Phi_M^{surf} = A_s\left[\sum M_i \hat{\mu}_i^f \frac{\partial \Gamma_i}{\partial t} - \rho_{surf}\hat{s}_{surf}\frac{\partial T}{\partial t} - \frac{\partial \rho_{surf}\hat{\psi}_{surf}}{\partial t}\right] \tag{64}$$

$$\Phi_M^f = \rho_f \phi \left[-p \frac{\partial}{\partial t}\left(\frac{1}{\rho_f}\right) + \sum \hat{\mu}_i^f \frac{\partial \hat{X}_i^f}{\partial t} - \hat{s}_f \frac{\partial T}{\partial t} - \frac{\partial \hat{\psi}_f}{\partial t} \right] \tag{65}$$

are the solid, surface and fluid part of the material dissipation, respectively. Here we limit the discussion to reversible responses (i.e. $\Phi_M = 0$) and the important subject of material inelasticity will be pursued elsewhere. The constitutive response of each phase must also be non-dissipative (i.e. $\Phi_M^s = 0$, $\Phi_M^{surf} = 0$ and $\Phi_M^f = 0$).

4.1 State equations of the fluid

Substituting $\Phi_M^f = 0$ and $\hat{\psi}_f = \hat{\psi}_f\left(1/\rho_f, T, \hat{X}_1^f, ..., \hat{X}_k^f\right)$ into Eq. (65) gives the free energy balance for the fluid mixture:

$$\left[p + \frac{\partial \hat{\psi}_f}{\partial\left(1/\rho_f\right)} \right] d\left(\frac{1}{\rho_f}\right) + \left(\hat{s}_f + \frac{\partial \hat{\psi}_f}{\partial T} \right) dT - \sum \left(\hat{\mu}_i^f - \frac{\partial \hat{\psi}_f}{\partial \hat{X}_i^f} \right) d\hat{X}_i^f = 0 \tag{66}$$

This holds for arbitrary increments of $\left(1/\rho_f, T, \hat{X}_1^f, ..., \hat{X}_k^f\right)$, giving the fluid state equations:

$$p = -\left.\frac{\partial \hat{\psi}_f}{\partial\left(1/\rho_f\right)}\right|_{T, \hat{X}_1^f, ..., \hat{X}_k^f}; \hat{s}_f = -\left.\frac{\partial \hat{\psi}_f}{\partial T}\right|_{\rho_f, \hat{X}_1^f, ..., \hat{X}_k^f}; \hat{\mu}_i^f = \left.\frac{\partial \hat{\psi}_f}{\partial \hat{X}_i^f}\right|_{\rho_f, T} \tag{67}$$

Other forms of state equations based on $\hat{e}_f$, $\hat{h}_f$ and $\hat{g}_f$ can be obtained through Legendre transformations as shown in Appendix 2.

4.2 Gibbs adsorption isotherm

Combining Eq. (64) with $\Phi_M^{surf} = 0$ gives the free energy balance for the surface:

$$d\psi_{surf} = \sum \mu_i^f d\Gamma_i^{surf} - s_{surf} dT \tag{68}$$

where $\psi_{surf} = \rho_{surf} \hat{\psi}_{surf}$, $\mu_i^f = M_i \hat{\mu}_i^f$ and $s_{surf} = \rho_{surf} \hat{s}_{surf}$. Perform Legendre transformation of ψ_{surf} with respect to Γ_i^{surf}:

$$\gamma\left(T, \mu_1^f, ..., \mu_k^f\right) = \psi_{surf}\left(T, \Gamma_1^{surf}, ..., \Gamma_k^{surf}\right) - \sum \mu_i^f \Gamma_i^{surf} \tag{69}$$

The physical meaning of γ can be inspected by converting Eq. (69) to extensive quantities. For this purpose, consider an unstretchable interface $\mathcal{A}_0'$ (the prime is used to distinguish it from $\mathcal{A}$ the interfacial area contained in Ω_t) as shown in Fig. 2a. In this case, the surface can only grow by cleavage or adding new molecules on both side of the surface, after which its area becomes $\mathcal{A}'$. Denoting $\mathcal{F}'_{surf} = \mathcal{A}' \psi_{surf}$ as the extensive surface Helmholtz free energy, we have:

$$d\mathcal{F}'_{surf} = \mathcal{A}'\, d\psi_{surf} + \psi_{surf}\, d\mathcal{A}' \tag{70}$$

Substitute Eqs. (68) and (69) into (70) and consider isothermal condition:

$$d\mathcal{F}'_{surf} = \gamma d\mathcal{A}' + \sum \mu_i^f\, d\mathcal{N}'^{surf}_i \tag{71}$$

where $\mathcal{N}'^{surf}_i = \mathcal{A}'\Gamma_i^{surf}$. The first term on the RHS of Eq. (71) characterize the work done in creating an infinitesimal surface $d\mathcal{A}'_{new}$ (Fig. 2b), and thus γ represents *surface energy* carried by a unit surface area. γ is also called *surface tension* to emphasize its role as the work-conjugated force of $d\mathcal{A}'$. Eq. (71) can be integrated along a specific path that the number of mole $\mathcal{N}'^{surf}_i$ and surface $\mathcal{A}'$ are added to an initially empty system at constant surface tension and molar composition (i.e. constant μ_i) (DeHoff, 2006):

$$\mathcal{F}'_{surf}\left(\mathcal{A}', \mathcal{N}'^{surf}_1, ..., \mathcal{N}'^{surf}_k\right) = \gamma\left(\mu_1^f, ..., \mu_k^f\right)\mathcal{A}' + \sum \mu_i^f\, \mathcal{N}'^{surf}_i \tag{72}$$

The celebrated Gibbs adsorption isotherm is derived by subtracting (71) from the total differential of (72):

$$d\gamma = -\sum \Gamma_i^{surf}\, d\mu_i^f \tag{73}$$

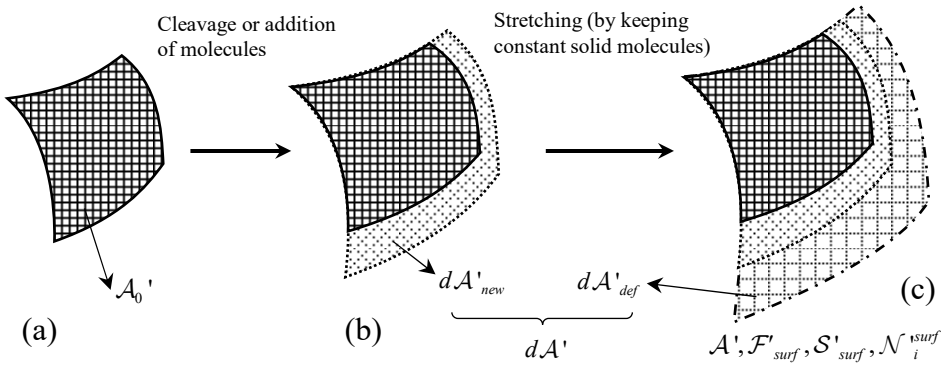

Fig. 2: Schematic of a deformable interface

4.3 Shuttleworth's equation

If the surface is deformable, another way of increasing the surface area is to stretch the solid surface $d\mathcal{A}'_{def}$ without adding new molecules or creating rupture, as illustrated in Fig. 2c. Such stretch can be measured by the logarithmic surface strain (Kramer and Weissmüller, 2007):

$$\varepsilon_A = \ln\left(\frac{\mathcal{A}'}{\mathcal{A}_0'}\right) \tag{74}$$

, giving $d\varepsilon_A = d\mathcal{A}'/\mathcal{A}'$. The deformation of the adsorbents can change the intermolecular distance of the adsorbates and consequently alter the surface energy. It is therefore natural to have ε_A enter the list of arguments of γ, revising Eq. (72) into:

$$\mathcal{F}'_{surf}\left(\mathcal{A}', \varepsilon_A, \mathcal{N}'^{surf}_1, ..., \mathcal{N}'^{surf}_k\right) = \gamma\left(\varepsilon_A, \mu_1^f, ..., \mu_k^f\right)\mathcal{A}' + \sum_i \mu_i^f\, \mathcal{N}'^{surf}_i \tag{75}$$

Substituting (74) into the total differential of (75) yields:

$$d\mathcal{F}'_{surf} = \sigma^s d\mathcal{A}' + \sum_i \mu_i^f d\mathcal{N}'^{surf}_i \tag{76}$$

where

$$\sigma^s\left(\varepsilon_A, \mu_1^f, ..., \mu_k^f\right) = \gamma\left(\varepsilon_A, \mu_1^f, ..., \mu_k^f\right) + \left.\frac{\partial\gamma\left(\varepsilon_A, \mu_1^f, ..., \mu_k^f\right)}{\partial\varepsilon_A}\right|_{\mu_1^f, ..., \mu_k^f} \tag{77}$$

is the so-called *surface stress* serving as the work-conjugated force of $d\mathcal{A}'$ for deformable surfaces. Apparently, σ^s reduces to γ for unstretchable interfaces where γ is independent of ε_A. Eq. (77) is known as the Shuttleworth's equation (Shuttleworth, 1950). Taking the partial derivative of (76) with respect to $\mathcal{A}'$ and using definition (74) gives:

$$\sigma^s\left(\varepsilon_A, \mu_1^f, ..., \mu_k^f\right) = \psi_{surf}\left(\varepsilon_A, \Gamma_1^{surf}, ..., \Gamma_k^{surf}\right) - \sum_i \mu_i \Gamma_i^{surf} \tag{78}$$

This implies that ψ_{surf} and σ^s are the Legendre transform of each other for deformable interfaces. The proposition of $\gamma = \gamma\left(\varepsilon_A, \mu_1^f, ..., \mu_k^f\right)$ also revises the Gibbs isotherm (73) in the following form (Eriksson, 1969):

$$d\gamma = -\sum \Gamma_i^{surf}(\varepsilon_A, \mu_1^f, ..., \mu_k^f) d\mu_i^f + \Pi^{surf} d\varepsilon_A \tag{79}$$

where $\Pi^{surf} = \left(\partial\gamma / \partial\varepsilon_A\right)\Big|_{\mu_1^f, ..., \mu_k^f} = \sigma^s - \gamma$. The dependency of Γ_i^{surf} on ε_A implies a two-way coupling between adsorption and deformation, which has received much attention lately (Do et al., 2008; Shen and Siderius, 2014).

4.4 Free energy balance of solid phase

The last term on the RHS of Eq. (63) accounts for the free energy change related to the kinetics of adsorption. Similar term also appears for reactive fluid mixtures (Coussy, 2010, Eq. 2.98). To focus on non-dissipative processes $\Phi_M^s = 0$, we consider a near-equilibrium scenario where adsorption occurs in a quasi-static manner (i.e. $\hat{\mu}_i^{surf} \approx \hat{\mu}_i^f$). Eq. (63) becomes after substituting Eq. (78) and $\Psi_s = \rho_s\left(1-\phi\right)\hat{\psi}_s$:

$$d\Psi_s = \mathbf{S} : d\mathbf{E} + p d\phi - S_s dT - \sigma^s dA_s \tag{80}$$

Comparing to the free energy balance of non-reactive porous solid (Coussy et al., 1998a), the specific surface area A_s now enters the macroscopic Ψ-potential, thus permitting the surface properties affect the thermomechanical response of the porous solid.

For isothermal, infinitesimal deformation processes (i.e. $\left\|\nabla\mathbf{u}^s\right\| \ll 1$), it is possible to neglect geometrical nonlinearity and write Eq. (80) as:

$$d\Psi_s = \overbrace{\sigma d\varepsilon + \mathbf{s}:d\mathbf{e} + pd\phi}^{df_s} - \overbrace{\sigma^s dA_s}^{du_{surf}} \tag{81}$$

where $\boldsymbol{\varepsilon} = \left(\nabla \mathbf{u}^s + {}^t\nabla \mathbf{u}^s\right)/2$ is the linearized strain tensor; $\varepsilon = \mathrm{tr}(\boldsymbol{\varepsilon})$ and $\mathbf{e} = \boldsymbol{\varepsilon} - \mathrm{tr}(\boldsymbol{\varepsilon})\mathbf{I}/3$ are the volumetric strain and strain deviator, respectively; $\sigma = \mathrm{tr}(\boldsymbol{\sigma})/3$ and $\mathbf{s} = \boldsymbol{\sigma} - \mathrm{tr}(\boldsymbol{\sigma})\mathbf{I}/3$ are the mean stress and stress deviator, respectively. Geometrically, A_s characterizes the inner structure of the porous medium and may be hypothesized as a function of the total strain and porosity (i.e. $A_s = A_s\left(\varepsilon, \mathbf{e}, \phi\right)$). Therefore, integration of Eq. (81) leads to the following form of Ψ_s:

$$\Psi_s = \Psi_s(\varepsilon, \mathbf{e}, \phi) = f_s(\varepsilon, \mathbf{e}, \phi) - u_{surf}(\varepsilon, \mathbf{e}, \phi) \tag{82}$$

Eq. (82) turns out to be identical to Eq. (1) which is frequently invoked to formulate adsorption-swelling models (Li and Feng, 2016; Vandamme et al., 2010). The present derivation, starting by explicitly listing the balance laws for the surface phase, provides a rigorous physical and mathematical basis of such hypothesis. It also confirms that the independent variables of u_{surf} contain only the state variables of the solid $\left(\varepsilon, \mathbf{e}, \phi\right)$ (or equivalently A_s). Indeed, u_{surf} defined by Eq. (81) should be carefully distinguished from the surface Helmholtz free energy ψ_{surf} in Eq. (68). The former should be regarded as a *surface strain energy density* that measures the accumulative elastic energy storage in a stretched surface, while the latter is the *surface Helmholtz free energy density* that serves as the true potential defining the state equations of the surface phase. For this difference, the appearance of only solid state variables in u_{surf} does not create any inconsistency, knowing that σ^s is not defined through such energy term but instead from the surface free energy via (76).

It is worth mentioning that the above derivations have the prerequisite that the porosity and the surface area can be clearly defined, i.e. for macroporous (pore size greater than 50 nm) and mesoporous (pore size between 2 nm to 50 nm) medium. Fluid molecules confined in micropores with size less than 2 nm interact with all the atoms of the pore surface, thus represents a very different micromechanical picture. The notions of surface area and porosity also become ambiguous in this case. Brochard et al. (2012) has proposed a macroscale theory applicable for generic pore size distributions including micropores. The key step is to replace the terms accounting for the free energy change attributed by fluid flux in mesoporous solids (i.e. $pd\phi + \sigma^s dA_s$) by a unified term (i.e. $\mu_i dn_i$) without distinguishing the host of these fluid molecules. In this way, the microporous solid is essentially treated as a solid mixture, with the details of the pore structure and molecular interactions within the pores neglected. Such generalization can be similarly pursued in the current framework by replacing the balance equations of the separate solid and surface phases with those of a single solid mixture that can interact with the fluid mixture. This goal will be pursued elsewhere. In the following, we approximate coal as a mesoporous solid, as similarly done by Vandamme et al. (2010), to inspect the capacities and limitations of current theory in modelling adsorption-induced deformations. This requires the specification of 1) the elastic model of coal matrix; 2) the microstructure of coals; 3) the adsorption isotherm of the gas mixture.

5 ADSORPTION-INDUCED SWELLING OF COALS

5.1 Isotropic and cross anisotropic poroelasticity

The following expression of Ψ_s corresponds to the linear isotropic poroelasticity:

$$\Psi_s(\varepsilon,\mathbf{e},\phi)=\frac{1}{2}\left(K+b^2N\right)\varepsilon^2-bN\varepsilon\left(\phi-\phi_0\right)+\frac{1}{2}N\left(\phi-\phi_0\right)^2+G\mathbf{e}:\mathbf{e} \tag{83}$$

where K and G are bulk and shear modulus, respectively; b and N are Biot's coefficient and Biot's modulus, respectively. Substituting (83) into (81) gives:

$$\begin{aligned}
\sigma-\sigma_a&=\left.\frac{\partial\Psi_s}{\partial\varepsilon}\right|_{\phi,\mathbf{e}}=\left(K+b^2N\right)\varepsilon-bN\left(\phi-\phi_0\right)\\
p-p_a&=\left.\frac{\partial\Psi_s}{\partial\phi}\right|_{\varepsilon,\mathbf{e}}=-bN\varepsilon+N\left(\phi-\phi_0\right)\\
\mathbf{s}&=\left.\frac{\partial\Psi_s}{\partial\mathbf{e}}\right|_{\varepsilon,\phi}=2G\mathbf{e}
\end{aligned} \tag{84}$$

where

$$\sigma_a=\sigma^s\left.\frac{\partial A_s}{\partial\varepsilon}\right|_{\phi,\mathbf{e}}\ \text{and}\ \ p_a=\sigma^s\left.\frac{\partial A_s}{\partial\phi}\right|_{\varepsilon,\mathbf{e}} \tag{85}$$

are the stress components contributed by surface tension and are referred to as *adsorption stresses*. It is assumed that such effect is isotropic and the stress deviator is unaffected. Alternatively, a cross anisotropic model can be obtained using the following expression of Ψ_s:

$$\begin{aligned}
\Psi_s(\varepsilon_{ij},\phi)&=\frac{1}{2}\left(c_{11}+b^2N\right)\left({\varepsilon_{11}}^2+{\varepsilon_{22}}^2\right)+\frac{1}{2}\left(c_{33}+{b_3}^2N\right){\varepsilon_{33}}^2\\
&+\left(c_{13}+b_3bN\right)\left(\varepsilon_{11}\varepsilon_{33}+\varepsilon_{22}\varepsilon_{33}\right)+\left(c_{12}+b^2N\right)\varepsilon_{11}\varepsilon_{22}\\
&+\frac{1}{2}\left(c_{11}-c_{12}\right){\varepsilon_{12}}^2+\frac{1}{2}c_{44}{\varepsilon_{13}}^2+\frac{1}{2}c_{44}{\varepsilon_{23}}^2\\
&-\left[b\left(\varepsilon_{11}+\varepsilon_{22}\right)+b_3\varepsilon_{33}\right]N\left(\phi-\phi_0\right)+\frac{1}{2}N\left(\phi-\phi_0\right)^2
\end{aligned} \tag{86}$$

where c_{11}, c_{12}, c_{13}, c_{33} and c_{44} are stiffness parameters; b_3 is the Biot's coefficient along the $\mathbf{e}_3$-direction. The corresponding constitutive equations can be expressed in compliance form:

$$\begin{bmatrix}\varepsilon_{11}\\ \varepsilon_{22}\\ \varepsilon_{33}\\ \varepsilon_{23}\\ \varepsilon_{13}\\ \varepsilon_{12}\\ \phi-\phi_0\end{bmatrix}=\begin{bmatrix}\frac{1}{E} & -\frac{\nu}{E} & -\frac{\nu_3}{E_3} & 0 & 0 & 0 & 0\\ -\frac{\nu}{E} & \frac{1}{E} & -\frac{\nu_3}{E_3} & 0 & 0 & 0 & 0\\ -\frac{\nu_3}{E_3} & -\frac{\nu_3}{E_3} & \frac{1}{E_3} & 0 & 0 & 0 & 0\\ 0 & 0 & 0 & \frac{1}{2G_3} & 0 & 0 & 0\\ 0 & 0 & 0 & 0 & \frac{1}{2G_3} & 0 & 0\\ 0 & 0 & 0 & 0 & 0 & \frac{1+\nu}{E} & 0\\ \frac{b-b\nu}{E}-\frac{b_3\nu_3}{E_3} & \frac{b-b\nu}{E}-\frac{b_3\nu_3}{E_3} & \frac{b_3}{E_3}-\frac{2b\nu_3}{E_3} & 0 & 0 & 0 & \frac{1}{N}\end{bmatrix}\begin{bmatrix}\sigma'_{11}\\ \sigma'_{22}\\ \sigma'_{33}\\ \sigma'_{23}\\ \sigma'_{13}\\ \sigma'_{12}\\ p-p_a\end{bmatrix} \tag{87}$$

where

$$\sigma'_{ij} = \sigma_{ij} + b_i\left(p - p_a\right)\delta_{ij} - \sigma_{ai}\delta_{ij} \text{ (no summation over } i\text{)} \tag{88}$$

may be regarded as the effective stress for saturated adsorptive porous media; $b_1 = b_2 = b, \sigma_{a1} = \sigma_{a2} = \sigma_a$ and

$$\sigma_a = \sigma^s \left.\frac{\partial A_s}{\partial \varepsilon_{11}}\right|_{\varepsilon_{33},\phi} = \sigma^s \left.\frac{\partial A_s}{\partial \varepsilon_{22}}\right|_{\varepsilon_{33},\phi};\ \sigma_{a3} = \sigma^s \left.\frac{\partial A_s}{\partial \varepsilon_{33}}\right|_{\varepsilon_{11},\phi};\ p_a = \sigma^s \left.\frac{\partial A_s}{\partial \phi}\right|_{\varepsilon_{11},\varepsilon_{33}} \tag{89}$$

The relations between parameters ($c_{11}, c_{12}, c_{13}, c_{33}, c_{44}$) and ($E, E_3, \nu, \nu_3, G_3$) are given by Abousleiman and Cui (1998). Experimental determinations of these parameters are discussed in other works (Loret et al., 2001; Rice and Cleary, 1976; Thompson and Willis, 1991). The closed-form constitutive model requires explicit expressions of the surface stress $\sigma^s\left(\varepsilon_A, \mu_1^f, ..., \mu_k^f\right)$ and the structural factors $\partial A_s / \partial \varepsilon_{11}\big|_{\varepsilon_{33},\phi}$, $\partial A_s / \partial \varepsilon_{33}\big|_{\varepsilon_{11},\phi}$ and $\partial A_s / \partial \phi\big|_{\varepsilon_{11},\varepsilon_{33}}$. They depend on the characteristics of the solid-fluid interface as well as the porous structure of the material.

5.2 Microstructure of coal

Coal exhibits complex microstructures at different length scales. For example, Australian coal contains micropores (0.01~0.05 μm in diameter), interbeded with micro and macro fractures (0.5~20 μm and 100~2000 μm in width respectively), and surrounded by wide cleats (5-60mm) (Gamson et al., 1993). Dull coals is rather dominated by microcavities with phyterial origins formed from fragments of plants. They typically resemble the structures of wood fibres characterized by long cylindrical cell lumen with outer diameters of 2-4 μm (Fig.3 a-c) (Gamson et al., 1996). Two types of idealized microstructures are analyzed here. The first type is characterized by uniformly distributed mono-sized spherical pores, which corresponds to a macroscopically isotropic poroelastic media. The second type, inspired by the phyterial structure of Dull coals, is idealized as arrays of thick-wall cylinders aligned along $\mathbf{e}_3$-axis with both ends closed so that the inner pore space and the outer space are isolated (Fig.3 d-f). Such structure corresponds to a macroscopically cross anisotropic poroelastic material.

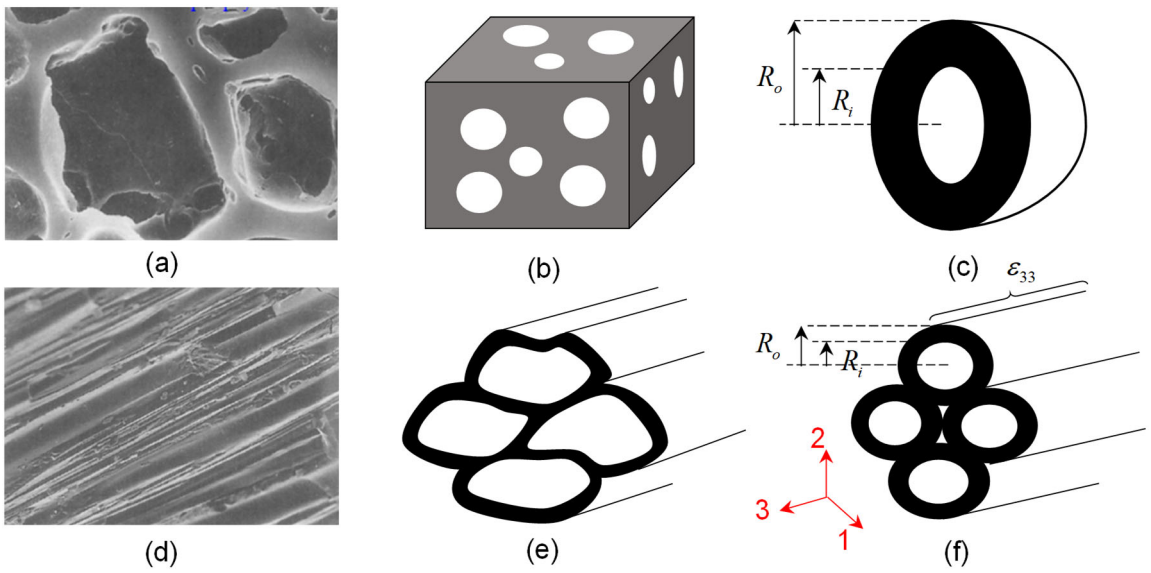

Fig. 3: (a) and (d) are the scanning electron microscope (SEM) of phyterial microstructures of coals (Gamson et al., 1996); (b) and (e) present the schematics of these microstructures; (c) and (f) illustrate the idealized thick-wall spheres and cylinders corresponding to each structures.

Spherical microstructure: The same microstructure has been studied by Vandamme et al. (2010). Here we present a slightly different derivation by treating the initial pore radius as a model parameter. Observing Fig. 3c, The initial and current porosity can be computed by:

$$\phi_0 = \frac{R_i^3}{R_o^3};\ \phi = \frac{\left(R_i + \Delta R_i\right)^3}{R_o^3} \tag{90}$$

where R_i is the inner and R_o is the outer radius of the sphere; ΔR_i is the change of the pore radius. A_s can be similarly expressed after eliminating R_o and ΔR_i using Eq. (90)

$$A_s = \frac{3\left(R_i + \Delta R_i\right)^2}{R_o^3} = \frac{3}{R_i}\phi_0^{1/3}\phi^{2/3} \tag{91}$$

The structural factors can be immediately derived:

$$\left.\frac{\partial A_s}{\partial \varepsilon}\right|_{\phi,\mathbf{e}} = 0;\ \left.\frac{\partial A_s}{\partial \phi}\right|_{\varepsilon,\mathbf{e}} = \frac{2}{R_i}\left(\frac{\phi_0}{\phi}\right)^{1/3} \tag{92}$$

Cylindrical microstructure: The elongation along $\mathbf{e_3}$ need to be considered in this scenario:

$$\phi_0 = \frac{R_i^2}{R_o^2};\ \phi = \frac{\left(1+\varepsilon_{33}\right)\left(R_i + \Delta R_i\right)^2}{R_o^2} \tag{93}$$

Express A_s in terms of ϕ and ϕ_0:

$$A_s = \frac{2\left(1+\varepsilon_{33}\right)\left(R_i+\Delta R_i\right)}{{R_o}^2} = \frac{2}{R_i}\sqrt{\left(1+\varepsilon_{33}\right)\phi_0\phi} \tag{94}$$

The structural factors become:

$$\left.\frac{\partial A_s}{\partial \varepsilon_{11}}\right|_{\varepsilon_{33},\phi} = \left.\frac{\partial A_s}{\partial \varepsilon_{22}}\right|_{\varepsilon_{33},\phi} = 0\,;\ \left.\frac{\partial A_s}{\partial \varepsilon_{33}}\right|_{\varepsilon_{11},\phi} = \frac{1}{R_i}\sqrt{\frac{\phi_0\phi}{\left(1+\varepsilon_{33}\right)}}\,;\ \left.\frac{\partial A_s}{\partial \phi}\right|_{\varepsilon_{11},\varepsilon_{33}} = \frac{1}{R_i}\sqrt{\frac{\left(1+\varepsilon_{33}\right)\phi_0}{\phi}} \tag{95}$$

Note that Eq. (92) should be used together with the isotropic model (84) while (95) should be paired with the cross anisotropic model (87) to maintain consistency between the assumed microstructures and the macroscopic behaviours.

5.3 Swelling induced by adsorption of pure gas

Hol and Spiers (2012) conducted a series of swelling tests on Brzeszcze coal. Specimens are pressurized by Helium (an inert gas) and CO_2 (a highly adsorptive gas) separately. The volume change in response to Helium injection is attributed to poroelastic compaction only, while the swelling due to CO_2 injection reflects the net outcome of the adsorption-induced swelling and elastic compression. Comparison between the two results gives separately the evolution of adsorption and elastic strain component as a function of gas pressure. Their data is used here to test the performance of the proposed model. Assume the adsorption of pure CO_2 on coals obeys the Langmuir isotherm:

$$\Gamma_{\mathrm{CO_2}}^{surf} = \frac{\Gamma_{\mathrm{CO_2}}^{\max} B_{\mathrm{CO_2}} p}{1+B_{\mathrm{CO_2}} p} \tag{96}$$

where $\Gamma_{\mathrm{CO_2}}^{\max}$ and $B_{\mathrm{CO_2}}$ are adsorption parameters. In writing Eq. (96) we have assumed that surface strain ε_A is sufficiently small and its impact on isotherms can be neglected. The more general case of stretch-dependent adsorption will be discussed in the next section. Combining Eqs. (96), (79) and (77) yields:

$$\sigma^s = \sigma_0^s - RT\Gamma_{\mathrm{CO_2}}^{\max}\ln\left(1+B_{\mathrm{CO_2}} p\right) \tag{97}$$

where $\sigma_0^s = \gamma_0 + \partial\gamma_0 / \partial\varepsilon_A\big|_{\mu_1^f,\ldots,\mu_k^f}$ is the surface stress in vacuum, which is regarded as a material constant (i.e. linear variation of γ_0 with respect to ε_A).

The isotropic poroelastic-swelling model contains 9 parameters and the cross anisotropic one has 13 parameters. Their values can be constrained with the help of existing literature. Hol and Spiers (2012) reported the apparent bulk modulus of Brzeszcze coal 7.4 ~ 7.7 GPa. These values, however, should not be directly used in poroelastic models where the apparent bulk modulus also depends on the Biot's coefficient. Espinoza et al. (2014) reported a Young's modulus of 2.5 ~ 2.7 GPa and a Poisson's ratio of 0.2 ~ 0.27 for bituminous coals interpreted using a poroelastic model. Li and Feng (2016) calibrated Anderson 01 and Gilson 02 coal specimens and obtained K=2.0~2.5 GPa, b= 0.73 ~ 0.82 and N=10.3 ~ 17.1 GPa. Both micropores and mesopores present in coals, suggesting a range of R_i of 10^{-9} ~ 10^{-7} m. The initial porosity of coals varies between 1% to 15% depending on their geological origins (Gamson et al., 1996). The surface stress of coal in vacuum can be estimated from its fracture toughness. The mode I critical fracture intensity factor of different types of coals measured under different test configurations varies drastically from 0.0281

to 2.329 MPa$\times$m$^{0.5}$ (Zipf and Bieniawski, 1990), with the majority ranges between 0.1 to 0.4 MPa$\times$m$^{0.5}$. By assuming E=2.5GPa and ν=0.2, the surface energy computed using Irwin's relation $2\gamma_0 = G_{IC} = (1-\nu)K_{IC}^2 / E$ is 1.6 ~ 25.6 J/m^2. Keeping above ranges in mind, the poroelastic parameters are calibrated to best fit the elastic strain vs. CO_2 pressure data. The adsorption and microstructure parameters are calibrated based on the swelling strain vs. CO_2 pressure data. Theses parameters are summarized in Table 1.

Table 1: Parameters for the proposed poroelastic-swelling model

	Poroelasticity								Microstructure		Adsorption		
	K	ν	b	N	E_3	ν_3	b_3	G_3	R_i	ϕ_0	σ_0^s	$\Gamma_{CO_2}^{max}$	B_{CO_2}
	GPa			GPa				GPa	μm		J/m^2	mol/m^2	
Isotropic poroelasticity with spherical microstructure	3	0.1	0.6	10	-	-	-	-	0.025	0.1	10	4.5e-5	1e-4
Cross anisotropic poroelasticity with cylindrical microstructure	3	0.1	0.6	10	3	0.1	0.64	4	0.025	0.1	10	1.2e-4	1e-4

Fig. 4 compares the computed responses with the experimental data from Brzeszcze coal sample 364-2. The existence of a transition pressure where the specimen switch from swelling to compaction is successfully captured (Fig. 4a), although the variations of swelling strain along different directions cannot be described by the isotropic model. Fig. 4b confirms that such transition is a result of the competition between the adsorption swelling and elastic compaction. As expected, adsorption dominates at low CO_2 pressures (< 20 MPa) and produces an overall swelling response, while elastic compaction becomes important at higher pressure levels (20~100 MPa) as adsorption approaching to saturation. The computed swelling strain vs. absolute adsorption curve (Fig. 4c) only captures the first data point, and underpredicts the total adsorption at higher swelling strains. This is because the current theory cannot fully account for adsorption taken place in micropores, underestimating the total adsorption capacity of the coal matrix. An extension of the theory for microporous media with advanced adsorption isotherms may help remediate this issue. The cross anisotropic model can capture the different responses along $\mathbf{e}_1$ and $\mathbf{e}_3$ axis as shown in Fig. 5a. The same level of agreement is observed on the volumetric strain vs. pressure plane (Fig. 5b). Again, the model underpredicts the total amount of adsorbed molecules response at elevated pressure levels (Fig. 5c).

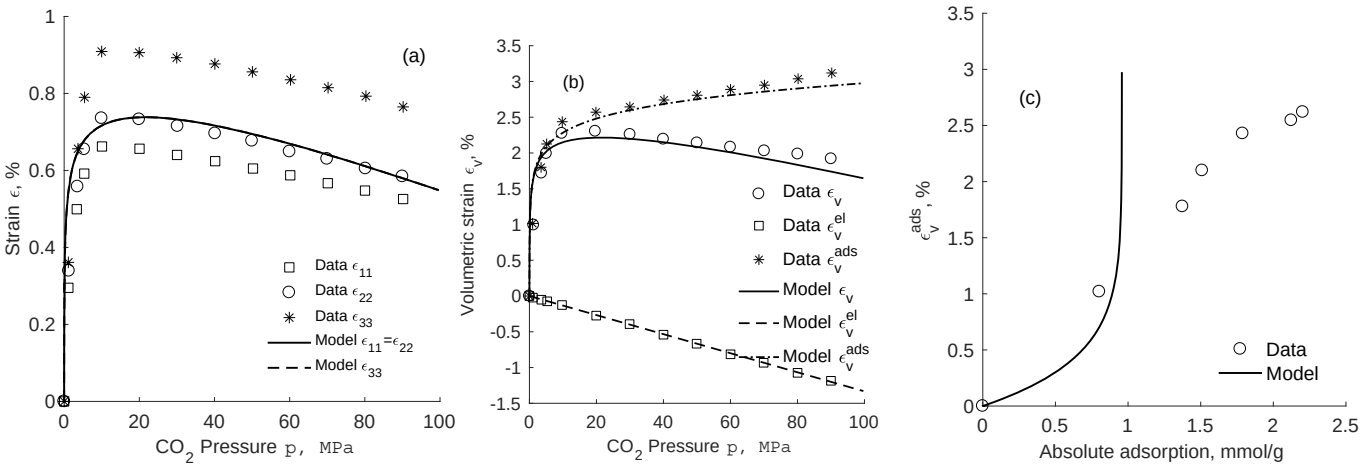

Fig. 4: Data vs. prediction using isotropic poroelastic model on a) strain components vs. pressure, b) volumetric strain vs. pressure and c) adsorption strain vs. absolute adsorption planes. A specific gravity G_s=1.35 is assumed for coal minerals in calculating the mole of adsorbed CO_2 per unit mass. Data from Hol and Spiers (2012).

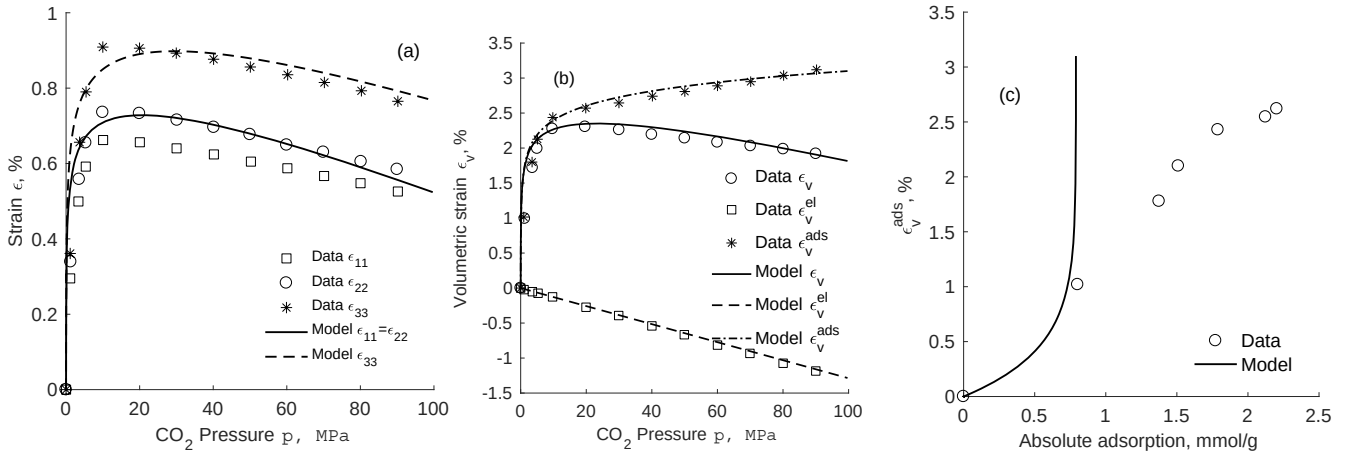

Fig. 5: Data vs. prediction using cross anisotropic poroelastic model on a) strain components vs. pressure, b) volumetric strain vs. pressure and c) adsorption strain vs. absolute adsorption planes. Data from Hol and Spiers (2012).

Espinoza et al. (2013) also matched the above dataset using a cross anisotropic model and a Langmuir-type isotherm within the microporous theory of Brochard et al. (2012). The derived adsorption stress can be isotropic, anisotropic or pressure-dependent, providing different levels of agreement with the experimental data. The current model differs from their approach in that the anisotropic adsorption stress is derived from the assumed cylindrical pores rather than assumed a priori. On the other hand, their approach does not require the notion of porosity or surface area, thus being more consistent with the microstructure of coals.

5.4 Swelling induced by adsorption of binary gas mixture

The adsorption of multicomponent gases may be described by the extended Langmuir model (Yang, 1987):

$$\Gamma_i^{surf} = \frac{\Gamma_i^{\max} B_i p_i}{1+\sum B_i p_i} \tag{98}$$

where $\Gamma_i^{\max}$ and B_i are adsorption parameters for pure gases; $p_i = X_i^f p$ is the partial pressure of component *i*. Day et al. (2012) reported the adsorption-swelling data of Australian coals in CO_2-CH_4 mixtures. Two types of tests have been conducted, one keeping constant gas composition and increasing the total pressure (Type I), the other maintaining constant total pressure and gradually altering the gas composition (Type II). Substituting Eq. (98) into (79) and (77) and integrating along the two CO_2 injection paths, one obtains:

$$\sigma^s(p, X^f_{\mathrm{CO}_2}) = \sigma^s_0 - RT\frac{\Gamma^{\max}_{\mathrm{CO}_2} B_{\mathrm{CO}_2} X^f_{\mathrm{CO}_2} + \Gamma^{\max}_{\mathrm{CH}_4} B_{\mathrm{CH}_4} X^f_{\mathrm{CH}_4}}{B_{\mathrm{CO}_2} X^f_{\mathrm{CO}_2} + B_{\mathrm{CH}_4} X^f_{\mathrm{CH}_4}} \ln\left(1 + \left(B_{\mathrm{CO}_2} X^f_{\mathrm{CO}_2} + B_{\mathrm{CH}_4} X^f_{\mathrm{CH}_4}\right) p\right) \tag{99}$$

for Type-I tests, and

$$\begin{aligned}\sigma^s(p, X^f_{\mathrm{CO}_2}) = \sigma^s_0 &+ RT\frac{\left(\Gamma^{\max}_{\mathrm{CO}_2} - \Gamma^{\max}_{\mathrm{CH}_4}\right) B_{\mathrm{CO}_2}}{B_{\mathrm{CO}_2} - B_{\mathrm{CH}_4}} \ln\left(1 + B_{\mathrm{CH}_4} p\right) \\ &- RT\frac{\Gamma^{\max}_{\mathrm{CO}_2} B_{\mathrm{CO}_2} - \Gamma^{\max}_{\mathrm{CH}_4} B_{\mathrm{CH}_4}}{B_{\mathrm{CO}_2} - B_{\mathrm{CH}_4}} \ln\left(1 + B_{\mathrm{CH}_4} p + (B_{\mathrm{CO}_2} - B_{\mathrm{CH}_4}) X^f_{\mathrm{CO}_2} p\right)\end{aligned} \tag{100}$$

for Type-II test. Their experiments did not separate the contributions of elastic compaction and adsorption swelling on the total volume changes, thus does not allow for the calibration of the poroelastic parameters. As a numerical example, we use the parameters for Brzeszcze coals and only modify the adsorption parameters to capture the two end-member scenarios (i.e. injection of pure CO_2 and CH_4). The volumetric responses in binary mixtures are then predicted by Eqs. (99) or (100) combined with the isotropic model. The predicted swelling curves for Type-I tests are presented in Fig. 6, showing excellent agreements with the experimental results at all CO_2 concentrations for both coal specimens (Coal A and Coal I).

Fig. 7a shows the model has well captured the slightly nonlinear swelling curve in Type-II tests. Fig. 7b compiles all the measured and predicted swelling strain as a function of CO_2 partial pressure obtained from different test paths. The experimental data shows that coal A reaches similar volumetric strains when fully saturated by CO_2 at the same pressure, and is independent of the way that CO_2 enters the specimen. Harpalani and Mitra (2010) has reported similar conclusions based on their study on Illinois and San Juan coal specimens. The model does not predict such convergence with the current set of parameters. Apparently, the extended Langmuir model gives a path-dependent surface stress, i.e. Eqs. (99) and (100) give different values of σ^s at $X^f_{\mathrm{CO}_2} = 1$ at the same *p*. The reason is that the extended Langmuir model is thermodynamically consistent only when the saturated adsorption $\Gamma_i^{\max}$ are the same for all components (Bai and Yang, 2001). In this case, the integrated σ^s is path independent only if $\Gamma^{\max}_{\mathrm{CO}_2} = \Gamma^{\max}_{\mathrm{CH}_4}$ (which can be easily checked comparing Eqs. (99) and (100)). This may be remediated in the future extensions of the theory by choosing advanced multicomponent adsorption models that are compatible with thermodynamics.

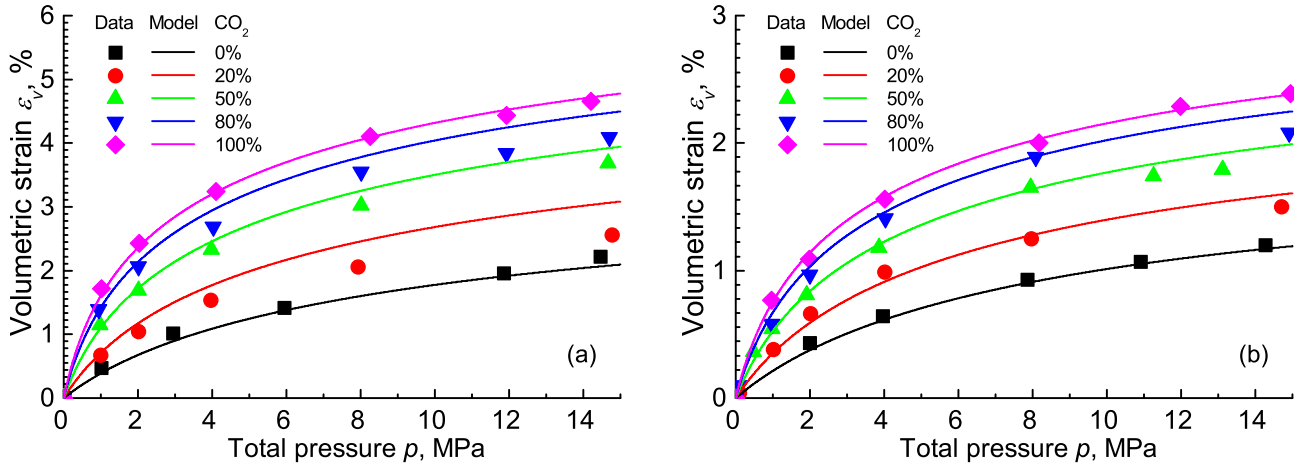

Fig. 6: Measured (Data from Day et al. (2012)) and predicted total strain during the injection of CO_2-CH_4 gas mixture in unconfined specimens of (a) Coal A and (b) Coal I. CO_2 concentrations are kept constant during injection. The adsorption parameters for Coal A are $\Gamma^{\max}_{CO_2}=3\times10^{-4}\,\text{mol/m}^2, B_{CO_2}=1\times10^{-6}, \Gamma^{\max}_{CH_4}=2\times10^{-4}\,\text{mol/m}^2, B_{CH_4}=4\times10^{-6}$ and for Coal I are $\Gamma^{\max}_{CO_2}=1.3\times10^{-4}\,\text{mol/m}^2, B_{CO_2}=1\times10^{-6}, \Gamma^{\max}_{CH_4}=1.1\times10^{-4}\,\text{mol/m}^2, B_{CH_4}=4\times10^{-6}$.

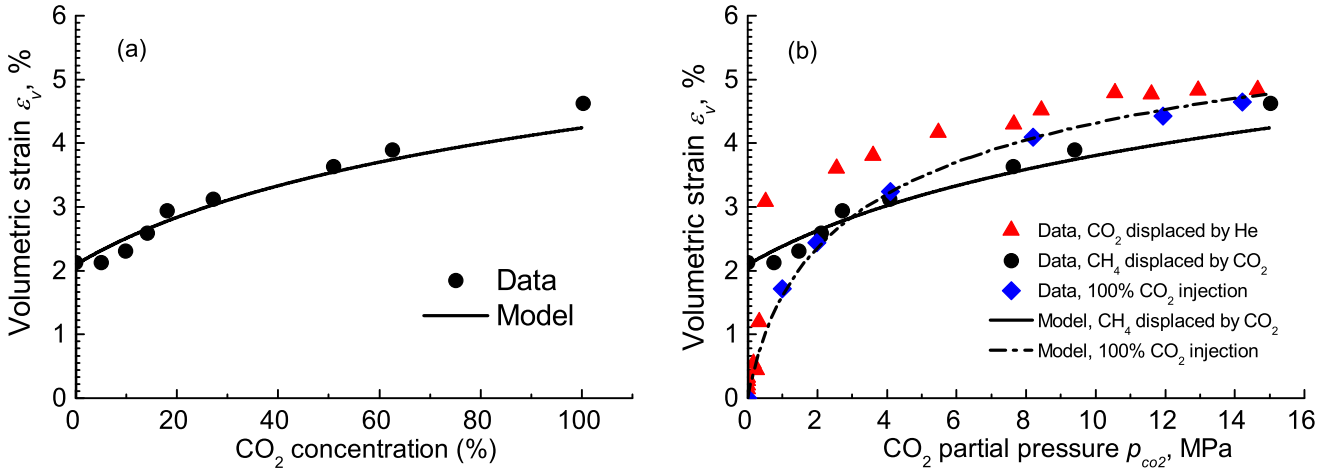

Fig. 7: Measured and predicted volumetric swelling of Coal A (a) during CO_2 injection of initially CH_4 -saturated specimen under constant total pressure p=15 MPa; (*b*) as a function of CO_2 partial pressure under different injection paths. Data from Day et al. (2012).

6 DISCUSSION

6.1 Coupling between adsorption and swelling

The previous analyses have assumed stretch-independent adsorption isotherms, consequently the derived γ and σ^s are independent of the deformation of the porous skeleton. This may be oversimplifying as the recent theoretical studies and numerical simulations have shown complex two-way coupling between the

adsorption characteristics and the deformation of adsorbents (Do et al., 2008; Gor and Bernstein, 2016; Shen and Siderius, 2014). To examine the implication of such coupling on the swelling behaviour of coals, it is possible to replace Eq. (96) with the following simple stretch-dependent adsorption model:

$$\Gamma_i^{surf}\left(\varepsilon_{A,}\mu_1^f,...,\mu_k^f\right)=\left(1+C\varepsilon_A\right)\Gamma_i^{surf,0}\left(\mu_1^f,...,\mu_k^f\right) \tag{101}$$

where C is the adsorption-stretch coupling constant. Considering pure CO_2 adsorption with $\Gamma_i^{surf,0}$ having the same form as (96), Eq. (79) becomes

$$d\gamma\left(\varepsilon_A,p\right)=-\left(1+C\varepsilon_A\right)RT\frac{\Gamma_{CO_2}^{\max}B_{CO_2}}{1+B_{CO_2}p}dp-CRT\Gamma_{CO_2}^{\max}\ln\left(1+B_{CO_2}p\right)d\varepsilon_A \tag{102}$$

where the Maxwell relation

$$\left.\frac{\partial\Gamma_{CO_2}^{surf}}{\partial\varepsilon_A}\right|_p=\left.\frac{\partial\Pi^{surf}}{\partial p}\right|_{\varepsilon_A} \tag{103}$$

has been invoked. Integrating (102) and substituting into (77) yields:

$$\sigma^s\left(\varepsilon_A,p\right)=\gamma_0-\left(1+2C\varepsilon_A\right)RT\Gamma_{CO_2}^{\max}\ln\left(1+B_{CO_2}p\right) \tag{104}$$

ε_A can be replaced by ε and ϕ using microstructural relations (91) and (94):

$$\varepsilon_A=\ln\frac{A_s}{A_{s0}}=\frac{2}{3}\ln\frac{\phi}{\phi_0}\ \text{ and }\ \varepsilon_A=\frac{1}{2}\ln\frac{\left(1+\varepsilon_{33}\right)\phi}{\phi_0} \tag{105}$$

for spherical and cylindrical microstructures, respectively. Fig. 8 presents the predicted total strain and absolute adsorption via Eq. (104). The Brzeszcze coal parameters are used again to give quantitative comparisons. It is observed that stronger coupling effect (i.e. higher C values) leads to larger swelling strain and higher adsorption capacity of the coal matrix. This is because more molecules can be adsorbed on the stretched pore surface (governed by Eq. (101)), giving lower surface stress and higher tendency to swell at the same CO_2 pressure. Fig. 8a shows that shape of the adsorption-swelling curve is also affected by the coupling effect. Specifically, higher C values postpone the point of swelling-contraction transition, and eventually diminish the contractive behaviour. Fig. 8b reveals that coupling become significant at CO_2 pressure 0.01 MPa. Beyond this point, the uncoupled model predicts that the adsorption approaches to saturation while the coupled model gives continuous increase in the total amount of adsorption.

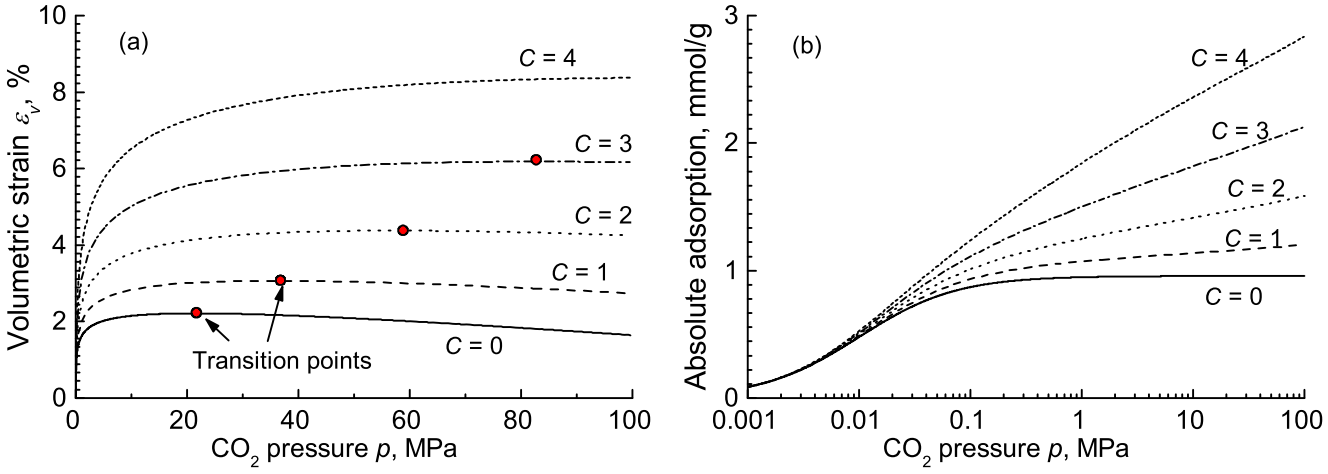

Fig. 8: Predicted (a) total strain and (b) absolute adsorption using different values of coupling constant C.

6.2 Adsorption-induced deformation of soft porous materials

Silica aerogels (a compliant, highly porous material) can reach up to 30% deformation when interacting with nitrogen (Reichenauer and Scherer, 2001). The proposed theory can be readily extended to account for geometrical nonlinearities in modeling soft porous materials interacting with adsorptive species. The first step is returning to the general free energy balance equation (80) and re-examining the adsorption characteristics (isotherms, surface stress, geometrical factors) under large deformations. The logarithmic measure of surface strain Eq. (74) holds regardless of the magnitude of stretching, thus can still be used as a state variable to represent the extent of surface deformation. The adsorption isotherms may be revised to have nonlinear dependency on ε_A (i.e. having C, $\Gamma_i^{\max}$ and B_i as functions of ε_A) if experimental data supports. This will also modify the expression of σ^s after integration. The geometrical factors for spherical microstructure remain the same as they are independent of strain. The cylindrical microstructure depends on ε_{33} and needs to be generalized. Defining stretch along $\mathbf{e}_3$ as $\Lambda_3 = dx_3 / dX_3$, Eq. (93) becomes:

$$\phi_0 = \frac{R_i^2}{R_o^2};\ \phi = \frac{\Lambda_3\left(R_i + \Delta R_i\right)^2}{R_o^2};\ A_s = \frac{2\Lambda_3\left(R_i + \Delta R_i\right)}{R_o^2} \tag{106}$$

, giving:

$$\left.\frac{\partial A_s}{\partial C_{11}}\right|_{C_{33},\phi} = \left.\frac{\partial A_s}{\partial C_{22}}\right|_{C_{33},\phi} = 0;\ \left.\frac{\partial A_s}{\partial C_{33}}\right|_{C_{11},\phi} = \frac{1}{2R_i} C_{33}^{-3/4}\sqrt{\phi_0\phi};\ \left.\frac{\partial A_s}{\partial \phi}\right|_{C_{11},C_{33}} = \frac{1}{R_i} C_{33}^{1/4}\sqrt{\frac{\phi_0}{\phi}} \tag{107}$$

where $\mathbf{C} = \mathbf{F}^T \cdot \mathbf{F}$ is the right Cauchy-Green tensor and $\Lambda_3 = \sqrt{C_{33}}$.

The last step is to specify the free energy $\Psi_s(\mathbf{E}, \phi)$ to derive a finite-strain constitutive law for the porous skeleton. We select the model by Nedjar (2013) to show an example of application, while other finite-strain poroelastic models can be straightforwardly adopted following the same procedure. The expression of Ψ_s proposed by Nedjar (2013) can be rewritten as:

$$\Psi_s\left(\mathbf{C},\phi\right)=\Psi'_s(\mathbf{C})+\Psi_s^{por}(J,\phi) \tag{108}$$

where

$$\Psi'_s(\mathbf{C})=\frac{K}{2}\left[\frac{1}{2}(J^2-1)-\ln J\right]+\frac{G}{2}\left(\bar{\mathbf{C}}:\mathbf{I}-3\right) \tag{109}$$

represents a compressible Neo-Hookean-type model;

$$\Psi_s^{por}(J,\phi)=N\left(\phi-\phi_0\right)-N(\phi-J)\ln\left[\frac{\phi-J}{H(J)-J}\right]+N\phi_0\left(1+m\right)\left(1-J\right) \tag{110}$$

embodies a nonlinear porosity law; $H(J)$ is defined as

$$H(J)=\begin{cases}\phi_0 J^m & \text{for } J\le 1\\ J-\left(J-\phi_0\right)\exp\left[\dfrac{\phi_0 m}{J-\phi_0}\left(J-1\right)\right] & \text{for } J>1\end{cases} \tag{111}$$

to ensure $n\to 0$ when $J\to 0^+$ and $n\to 1$ when $J\to+\infty$; K, G, N and m are material parameters; $\bar{\mathbf{C}}=J^{-2/3}\mathbf{C}$ is the volume-preserving right Cauchy-Green tensor. Substituting (108) into (80) leads to the closed-form constitutive equations:

$$\begin{aligned}\boldsymbol{\sigma}-\sigma_a\mathbf{I}&=\frac{K}{2}\left[J-\frac{1}{J}\right]\mathbf{I}+\frac{G}{J}\operatorname{dev}\bar{\mathbf{B}}+\frac{\partial\Psi_s^{por}}{\partial J}\mathbf{I}\\ p-p_a&=-N\ln\left[\frac{\phi-J}{H(J)-J}\right]\end{aligned} \tag{112}$$

where $\mathbf{B}=\mathbf{F}\cdot\mathbf{F}^T$ and $\bar{\mathbf{B}}=J^{-2/3}\mathbf{B}$ are the left Cauchy-Green tensor and its volume-preserving counterpart, respectively. To give a numerical example, let us consider again the unconfined gas pressurization test. The simple stretch-dependent adsorption model Eq. (101) is kept unchanged to focus more on geometrical nonlinearity. The Brzeszcze coal parameters are chosen as the baseline, with the poroelastic parameters adjusted to represent a compliant porous matrix. These parameters are also selected in such a way that the solution of (112) converges to that given by the linear model (84) near J = 1 and $\phi=\phi_0$ at the absence of adsorption stresses. The computed results with C=0 and C=0.3 are shown in Fig. 9a and b, respectively. Both models give the same elastic response J^{el} at low pressure but diverges as pressure increases. Apparently, the linear model does not provide a lower bound for J and negative value can occur. The adsorption deformation J^{ads} given by the nonlinear model is greater than the linear model, resulting in a neutral total volumetric deformation ($J\approx 1$) at large pressures. Fig. 9b demonstrates that the coupling effect amplifies the swelling strain and diminishes the contraction zone at elevated pressures. In summary, the incorporation of stretch-dependent adsorption model and geometrical nonlinearity can greatly affect the qualitative trend of adsorption-swelling curves predicted model. Therefore, they are important factors that demand more thorough experimental validations to be incorporated in modelling soft porous materials.

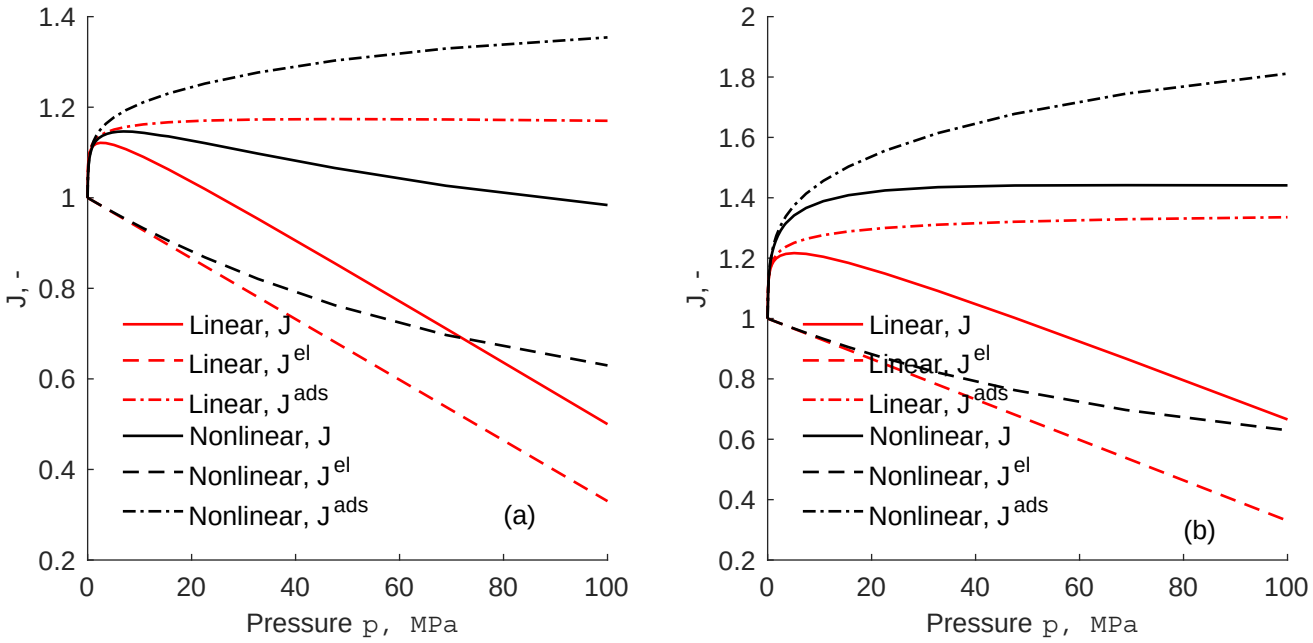

Fig. 9: Adsorption-deformation of a soft porous matrix with (a) C=0 and (b) C=0.3. Parameters for the linear model: K=10MPa, N=10MPa, b=0.33; for the nonlinear model: K=10MPa, N=10MPa, m=1. The rest of the parameters are the same as Table 1.

7 CONCLUSIONS

We have established a macroscopic theory for porous continua interacting with adsorptive fluid mixtures. The solid-fluid interface is treated as an independent phase that can carry mass, energy and entropy. The derivation starts with the fundamental balance laws from the mixture theory, with the contributions from the surface phase explicitly acknowledged. The derived Clausius-Duhem inequality embodies the coupled fluid, species and heat conduction laws, the state equations of the fluid, the Gibb's isotherm and the Shuttleworth's equation for the interface, and the constitutive equations for the solid skeleton. No assumption is made on the magnitude of deformation (i.e. finite strain) and the composition of the fluid (i.e. arbitrary number of species). Quantitative examples of application on coal swelling are discussed using different poroelastic models, microstructures, adsorption models, gas compositions and injection paths. Implications of stretch-dependent adsorption and finite-strain deformation of the skeleton are investigated. The main conclusions of this study are highlighted in the following:

1) The free energy decomposition Eq. (1) can be derived by explicitly listing the balance equations for the surface phase in the solid-surface-fluid system. We show that u_{surf} is the surface strain energy density that measures the elastic energy storage in the stretched surface while ψ_{surf} is the surface Helmholtz free energy that serves as the true potential defining the state equations of the surface phase.
2) Surface stress introduces a compressive prestress on the solid skeleton and thus installs a compressive volumetric strain prior to external loading. The magnitude of such prestress depends on the microstructure of the porous media and the surface tension of the solid-fluid interface. Swelling is a result of the reduction of the surface stress due to adsorption.
3) The model can separate the contribution of swelling strain and elastic strain on the total deformation of coal specimens during CO_2 pressurization. The transition from swelling to compaction as gas pressure increases can be successfully captured, confirming the competition roles between adsorption swelling

and elastic compaction. The cross anisotropic poroelasticity combined with the cylindrical microstructure also captures the different swelling response along different directions.

4) The use of extended Langmuir model allows for modelling adsorption-deformation in gas mixtures. Such generalization can well predict the volumetric behaviour of coal specimens under different CO_2-CH_4 injection paths. It does not capture the path-independent swelling suggested by experimental observations due to the thermodynamic inconsistency of the extended Langmuir model.
5) The use of stretch-dependent adsorption model introduces a two-way coupling between deformation and adsorption. If the porous material is highly compliant, geometrical nonlinearity must be considered as it can change the qualitative trend of the predicted adsorption-swelling responses. These factors require further in-depth theoretical studies and experimental validations.

APPENDIX

Appendix 1. Derivation of Eq. (32)

Eq. (35) can be rewritten by separating the work contribution by deformation and by inertial forces:

$$\mathcal{P}_{\mathbf{f},\mathbf{T}} = \mathcal{P}_{def} + \int_{\Omega_t} \left[\rho_s (1-n) \boldsymbol{\gamma}^s \cdot \mathbf{V}^s + \rho_{surf} a_s \mathbf{V}^s \cdot \boldsymbol{\gamma}^s + \rho_f n \mathbf{V}^f \cdot \boldsymbol{\gamma}^f \right] d\Omega_t \tag{113}$$

where $\mathcal{P}_{def}$ is the strain work rate:

$$\begin{aligned} \mathcal{P}_{def} &= \int_{\Omega_t} \left[\rho_s (1-n) \left(\mathbf{f} - \boldsymbol{\gamma}^s \right) \cdot \mathbf{V}^s + \rho_{surf} a_s \left(\mathbf{f} - \boldsymbol{\gamma}^s \right) \cdot \mathbf{V}^s + \rho_f n \left(\mathbf{f} - \boldsymbol{\gamma}^f \right) \cdot \mathbf{V}^f \right] d\Omega_t \\ &+ \int_{\partial\Omega_t} \left[\mathbf{T}^s \cdot \mathbf{V}^s + \mathbf{T}^s \cdot \mathbf{V}^s + \mathbf{T}^f \cdot \mathbf{V}^f \right] da \end{aligned} \tag{114}$$

The rate of change of kinetic energies can be simplified by applying mass balance equations:

$$\begin{aligned} \frac{d^s \mathcal{K}^s}{dt} &= \int_{\Omega_t} \left[\rho_s (1-n) \mathbf{V}^s \frac{d^s \mathbf{V}^s}{dt} + \frac{1}{2} \mathbf{V}^{s2} \overbrace{\left(\frac{d^s \rho_s (1-n)}{dt} + \rho_s (1-n) \nabla \cdot \mathbf{V}^s \right)}^{=0} \right] d\Omega_t = \int_{\Omega_t} \left(\rho_s (1-n) \mathbf{V}^s \cdot \boldsymbol{\gamma}^s \right) d\Omega_t \\ \frac{d^s \mathcal{K}^{surf}}{dt} &= \int_{\Omega_t} \left[\rho_{surf} A_s \mathbf{V}^s \frac{d^s \mathbf{V}^s}{dt} + \frac{1}{2} \mathbf{V}^{s2} \overbrace{\left(\frac{d^s \rho_{surf} a_s}{dt} + \rho_{surf} A_s \nabla \cdot \mathbf{V}^s \right)}^{=\hat{r}} \right] d\Omega_t = \int_{\Omega_t} \left(\rho_{surf} a_s \mathbf{V}^s \cdot \boldsymbol{\gamma}^s + \frac{1}{2} \mathbf{V}^{s2} \hat{r} \right) d\Omega_t \\ \frac{d^f \mathcal{K}^f}{dt} &= \int_{\Omega_t} \left[\rho_f n \mathbf{V}^f \frac{d^f \mathbf{V}^f}{dt} + \frac{1}{2} \mathbf{V}^{f2} \overbrace{\left(\frac{d^f \rho_f n}{dt} + \rho_f n \nabla \cdot \mathbf{V}^f \right)}^{=-\hat{r}} \right] d\Omega_t = \int_{\Omega_t} \left(\rho_f n \mathbf{V}^f \cdot \boldsymbol{\gamma}^f - \frac{1}{2} \mathbf{V}^{f2} \hat{r} \right) d\Omega_t \end{aligned} \tag{115}$$

Substituting Eq. (115) into (113) gives the *kinetic energy theorem* for adsorptive porous media:

$$\mathcal{P}_{\mathbf{f},\mathbf{T}} = \mathcal{P}_{def} + \frac{d^s \mathcal{K}^s}{dt} + \frac{d^s \mathcal{K}^{surf}}{dt} + \frac{d^f \mathcal{K}^f}{dt} + \int_{\Omega_t} \frac{1}{2}\left(\mathbf{V}^{f2} - \mathbf{V}^{s2}\right)\hat{r} d\Omega_t \tag{116}$$

Eq. (116) resembles the kinetic energy theorem for non-reactive porous solid (Coussy, 2004, Eq. 2.54). The two new terms are $d^s \mathcal{K}^{surf} / dt$ that accounts for the change of kinetic energy carried by the surface excess mass and the last term of Eq. (116) that accounts for the change of kinetic energy change due to adsorption. On the other hand, the strain work rate $\mathcal{P}_{def}$ can be simplified by substituting $\boldsymbol{\sigma} = \boldsymbol{\sigma}^s + \boldsymbol{\sigma}^{surf} + \boldsymbol{\sigma}^f$ and applying divergence theorem:

$$\mathcal{P}_{def} = \int_{\Omega_t} \left\{ \begin{array}{l} \boldsymbol{\sigma} : \mathbf{D} + \boldsymbol{\sigma}^f : \nabla_x \left(\mathbf{V}^f - \mathbf{V}^s\right) \\ + \left(\mathbf{V}^f - \mathbf{V}^s\right) \cdot \left[\nabla_x \cdot \boldsymbol{\sigma}^f + \rho_f n \left(\mathbf{f} - \boldsymbol{\gamma}^f\right)\right] \\ + \mathbf{V}^s \cdot \left[\nabla_x \cdot \boldsymbol{\sigma}^s + \rho_s (1-n)\left(\mathbf{f} - \boldsymbol{\gamma}^s\right)\right] \\ + \mathbf{V}^s \cdot \left[\nabla_x \cdot \boldsymbol{\sigma}^{surf} + \rho_{surf} a_s \left(\mathbf{f} - \boldsymbol{\gamma}^s\right)\right] \\ + \mathbf{V}^s \cdot \left[\nabla_x \cdot \boldsymbol{\sigma}^f + \rho_f n \left(\mathbf{f} - \boldsymbol{\gamma}^f\right)\right] \end{array} \right\} d\Omega_t \tag{117}$$

Substituting Eqs. (24)-(26) gives

$$\mathcal{P}_{def} = \int_{\Omega_t} \left[\boldsymbol{\sigma} : \mathbf{D} - \nabla_x \cdot \left[pn \left(\mathbf{V}^f - \mathbf{V}^s\right)\right] + \left(\mathbf{f} - \boldsymbol{\gamma}^f\right) \cdot \hat{\mathbf{w}} \right] d\Omega_t \tag{118}$$

Finally, substituting Eqs. (116) and (118) into Eq. (32), the kinetic energy terms on both side cancels out and the remainder can be written in the local form Eq. (38). The Lagrangian energy balance can be derived by integrating Eq. (38) with respect to the current configuration Ω_t:

$$\begin{aligned} \frac{d^s}{dt} \int_{\Omega_t} e d\Omega_t = & \int_{\Omega_t} \boldsymbol{\sigma} : \mathbf{D} d\Omega_t - \int_{\partial\Omega_t} \hat{h}_f \hat{\mathbf{w}} \cdot \mathbf{n} da + \int_{\Omega_t} \left(\mathbf{f} - \boldsymbol{\gamma}^f\right) \cdot \hat{\mathbf{w}} d\Omega_t \\ & - \sum \int_{\Omega_t} \left(\hat{\mu}_i^f - \hat{\mu}_i^{surf}\right) \hat{r}_i d\Omega_t - \int_{\partial\Omega_t} \mathbf{q} \cdot \mathbf{n} da - \sum \int_{\partial\Omega_t} \hat{\mu}_i^f \hat{\mathbf{h}}_i^f \cdot \mathbf{n} da \end{aligned} \tag{119}$$

, then pull back to the reference configuration Ω_0:

$$\begin{aligned} \frac{\partial}{\partial t} \int_{\Omega_0} E d\Omega_0 = & \int_{\Omega_0} \mathbf{S} : \frac{\partial \mathbf{E}}{\partial t} d\Omega_0 - \int_{\partial\Omega_0} \hat{h}_f \hat{\mathbf{W}} \cdot \mathbf{N} dA + \int_{\Omega_0} \left(\mathbf{f} - \boldsymbol{\gamma}^f\right) \cdot \mathbf{F} \cdot \hat{\mathbf{W}} d\Omega_0 \\ & - \sum \int_{\Omega_0} \left(\hat{\mu}_i^f - \hat{\mu}_i^{surf}\right) \hat{R}_i d\Omega_0 - \int_{\partial\Omega_0} \mathbf{Q} \cdot \mathbf{N} dA - \sum \int_{\partial\Omega_0} \hat{\mu}_i^f \hat{\mathbf{H}}_i^f \cdot \mathbf{N} dA \end{aligned} . \tag{120}$$

Eq. (39) immediately follows from Eq. (120).

Appendix 2. Energy potentials for homogenous multicomponent fluid

Consider a closed system with volume $\mathcal{V}_f$ occupied by a fluid mixture of *k* species. Its energy balance in terms of extensive quantities can be written as (DeHoff, 2006):

$$d\mathcal{E}_f = -pd\mathcal{V}_f + Td\mathcal{S}_f + \sum \hat{\mu}_i^f dM_i \mathcal{N}_i^f \tag{121}$$

Note we have used the mass-specific chemical potential $\hat{\mu}_i^f$ throughout this paper rather than the usual mole-specific chemical potential μ_i^f. The molar mass M_i in the last term of Eq. (121) is necessary to keep the unit consistent. The extensive quantities are related with intensive quantities by:

$$\mathcal{E}_f = \rho_f \mathcal{V}_f \hat{e}_f; \mathcal{S}_f = \rho_f \mathcal{V}_f \hat{s}_f; \mathcal{N}_i^f = \mathcal{V}_f n_i^f \tag{122}$$

Substituting Eq. (122) into (121) gives:

$$\rho_f \mathcal{V}_f d\hat{e}_f = T\rho_f \mathcal{V}_f d\hat{s}_f + \sum \hat{\mu}_i^f \mathcal{V}_f dM_i n_i^f + \left(T\hat{s}_f - \hat{e}_f\right)\mathcal{V}_f d\rho_f + \left(-p + T\rho_f \hat{s}_f + \sum M_i \hat{\mu}_i^f n_i^f - \rho_f \hat{e}_f\right) d\mathcal{V}_f \tag{123}$$

This must hold for an arbitrary control volume $d\mathcal{V}_f$. Thus, the last term on RHS must vanish:

$$\hat{e}_f = -p\left(\frac{1}{\rho_f}\right) + T\hat{s}_f + \sum \hat{\mu}_i^f \hat{X}_i^f \tag{124}$$

where $\hat{X}_i^f = M_i n_i / \rho_f$ for a homogenous system. With above relation, Eq. (123) can be simplified to

$$d\hat{e}_f = -pd\left(\frac{1}{\rho_f}\right) + Td\hat{s}_f + \sum \hat{\mu}_i^f d\hat{X}_i^f \tag{125}$$

Eq. (125) is consistent with Eq. (124). The other three energy potentials can be derived by performing Legendre transformation of $\hat{e}\left(1/\rho_f, \hat{s}_f, \hat{X}_1^f, ..., \hat{X}_k^f\right)$ with respect to $1/\rho_f$ and $\hat{s}_f$:

$$\hat{h}_f\left(p, \hat{s}_f, \hat{X}_1^f, ..., \hat{X}_k^f\right) = \hat{e}_f + p\frac{1}{\rho_f} = T\hat{s}_f + \sum \hat{\mu}_i^f \hat{X}_i^f \tag{126}$$

$$\hat{\psi}_f\left(\frac{1}{\rho_f}, T, \hat{X}_1^f, ..., \hat{X}_k^f\right) = \hat{e}_f - T\hat{s}_f = -p\frac{1}{\rho_f} + \sum \hat{\mu}_i^f \hat{X}_i^f \tag{127}$$

$$\hat{g}_f\left(p, T, \hat{X}_1^f, ..., \hat{X}_k^f\right) = \hat{e}_f + p\frac{1}{\rho_f} - T\hat{s}_f = \sum \hat{\mu}_i^f \hat{X}_i^f \tag{128}$$

The state equations can be derived in terms of $\hat{g}_f$ by substituting Eq. (128) into (125):

$$\frac{1}{\rho_f} = \left.\frac{\partial \hat{g}_f}{\partial p}\right|_{T, \hat{X}_1^f, ..., \hat{X}_k^f}, \ \hat{s}_f = -\left.\frac{\partial \hat{g}_f}{\partial T}\right|_{p, \hat{X}_1^f, ..., \hat{X}_k^f}, \ \hat{\mu}_i^f = \left.\frac{\partial \hat{g}_f}{\partial \hat{X}_i^f}\right|_{p,T} \tag{129}$$

The last equation of (129) is the usual definition of chemical potential (DeHoff, 2006). If the fluid mixture under consideration occupies the pore space of a solid skeleton with porosity ϕ, it is possible to show that the only difference in energy potentials is to update $\hat{X}_i^f$ with definition Eq. (18).

Appendix 3. Derivation of Eqs.* (47) *and (62)

Rearranging Eq. (45) gives:

$$\frac{\partial S}{\partial t}=\frac{1}{T}\left(\frac{\partial E}{\partial t}-\frac{\partial \Psi}{\partial t}-S\frac{\partial T}{\partial t}\right) \tag{130}$$

Substituting Eqs. (130) and (39) into (43), one obtains:

$$\begin{aligned}&\mathbf{S}:\frac{\partial \mathbf{E}}{\partial t}-\nabla_X\cdot\left[\hat{h}_f-T\hat{s}_f\right]\hat{\mathbf{W}}-\hat{s}_f\hat{\mathbf{W}}\cdot\nabla_X T\\&-\nabla_X\cdot\mathbf{Q}+\left(\mathbf{f}-\boldsymbol{\gamma}^f\right)\cdot\mathbf{F}\cdot\hat{\mathbf{W}}-\sum\nabla_X\cdot\hat{\mu}_i^f\hat{\mathbf{H}}_i^f-\frac{\partial\Psi}{\partial t}-S\frac{\partial T}{\partial t}\\&-\sum\left(\hat{\mu}_i^f-\hat{\mu}_i^{surf}\right)\hat{R}_i+\nabla_X\cdot\mathbf{Q}-\frac{1}{T}\mathbf{Q}\cdot\nabla_X T\geq 0\end{aligned} \tag{131}$$

Applying Eqs. (127) and (128) gives:

$$\begin{aligned}&\mathbf{S}:\frac{\partial \mathbf{E}}{\partial t}-\hat{g}_f\nabla_X\cdot\hat{\mathbf{W}}-\sum\hat{\mu}_i^f\nabla_X\cdot\hat{\mathbf{H}}_i^f-S\frac{\partial T}{\partial t}-\frac{\partial\Psi}{\partial t}\\&+\left[-\nabla_X\hat{g}_f-\hat{s}_f\nabla_X T+\left(\mathbf{f}-\boldsymbol{\gamma}^f\right)\cdot\mathbf{F}\right]\cdot\hat{\mathbf{W}}-\sum\hat{\mathbf{H}}_i^f\cdot\nabla_X\hat{\mu}_i^f-\frac{\mathbf{Q}}{T}\cdot\nabla_X T-\sum\left(\hat{\mu}_i^f-\hat{\mu}_i^{surf}\right)\hat{R}_i\geq 0\end{aligned} \tag{132}$$

To further simplify Eq. (132), it is necessary to rewrite the species mole balance (11) and (12) and combine with the averaging relation (19)

$$\frac{d^s M_i\left(n_i^f+\Gamma_i^{surf}a_s\right)}{dt}+M_i\left(n_i^f+\Gamma_i^{surf}a_s\right)\nabla_x\cdot\mathbf{V}^s+\nabla_x\cdot\hat{X}_i^f\hat{\mathbf{w}}+\nabla_x\cdot\hat{\mathbf{h}}_i^f=0 \tag{133}$$

or

$$\frac{\partial M_i\left(N_i^f+\Gamma_i^{surf}A_s\right)}{\partial t}+\nabla_X\cdot\hat{X}_i^f\hat{\mathbf{W}}+\nabla_X\cdot\hat{\mathbf{H}}_i^f=0 \tag{134}$$

Multiply both sides by $\hat{\mu}_i^f$ and summing over *k*:

$$-\sum\hat{\mu}_i^f\hat{\mathbf{W}}\cdot\nabla_X\hat{X}_i^f-\sum\hat{\mu}_i^f\hat{X}_i^f\nabla_X\cdot\hat{\mathbf{W}}-\sum\hat{\mu}_i^f\nabla_X\cdot\hat{\mathbf{H}}_i^f=\sum\hat{\mu}_i^f\frac{\partial M_i\left(N_i^f+\Gamma_i^{surf}A_s\right)}{\partial t} \tag{135}$$

Noticing $\hat{g}_f=\sum\hat{\mu}_i^f\hat{X}_i^f$ and the averaging relation (18), Eq. (135) becomes:

$$-\hat{g}_f\nabla_X\cdot\hat{\mathbf{W}}-\sum\hat{\mu}_i\nabla_X\cdot\hat{\mathbf{H}}_i^f=\hat{g}_f\frac{\partial\rho_f\phi}{\partial t}+\sum\rho_f\phi\hat{\mu}_i^f\frac{\partial\hat{X}_i^f}{\partial t}+\sum M_i\hat{\mu}_i^f\frac{\partial\Gamma_i^{surf}A_s}{\partial t}+\sum\hat{\mu}_i\hat{\mathbf{W}}\cdot\nabla_X\hat{X}_i^f \tag{136}$$

Substituting (136) into (132) yields:

$$\begin{aligned}&\mathbf{S}:\frac{\partial \mathbf{E}}{\partial t}+\hat{g}_f\frac{\partial \rho_f\phi}{\partial t}+\sum\rho_f\phi\hat{\mu}_i^f\frac{\partial \hat{X}_i^f}{\partial t}+\sum M_i\hat{\mu}_i^f\frac{\partial \Gamma_i^{surf}A_s}{\partial t}-\sum\left(\hat{\mu}_i^f-\hat{\mu}_i^{surf}\right)\hat{R}_i-S\frac{\partial T}{\partial t}-\frac{\partial \Psi}{\partial t}\\&+\left[-\nabla_X\hat{g}_f-\hat{s}_f\nabla_X T+\left(\mathbf{f}-\hat{\boldsymbol{\gamma}}^f\right)\cdot\mathbf{F}+\sum\hat{\mu}_i^f\nabla_X\hat{X}_i^f\right]\cdot\hat{\mathbf{W}}-\sum\hat{\mathbf{H}}_i^f\cdot\nabla_X\hat{\mu}_i^f-\frac{\mathbf{Q}}{T}\cdot\nabla_X T\geq 0\end{aligned}\tag{137}$$

Eq. (137) can be grouped into four relatively independent dissipation terms as expressed in Eq. (47). Among them, the material dissipation can be further simplified by decomposing S and Ψ via Eqs. (44) and (46):

$$\begin{aligned}\Phi_M=&\mathbf{S}:\frac{\partial \mathbf{E}}{\partial t}+p\frac{\partial \phi}{\partial t}-S_s\frac{\partial T}{\partial t}-\frac{\partial \rho_s(1-\phi)\hat{\psi}_s}{\partial t}+\left(\hat{g}_f-\hat{\psi}_f\right)\frac{\partial \rho_f\phi}{\partial t}-p\frac{\partial \phi}{\partial t}\\&+\sum M_i\hat{\mu}_i\frac{\partial \Gamma_i^{surf}A_s}{\partial t}-\rho_{surf}A_s\hat{s}_{surf}\frac{\partial T}{\partial t}-\frac{\partial \rho_{surf}A_s\hat{\psi}_{surf}}{\partial t}\\&+\sum\rho_f\phi\hat{\mu}_i\frac{\partial \hat{X}_i^f}{\partial t}-\rho_f\phi\hat{s}_f\frac{\partial T}{\partial t}-\rho_f\phi\frac{\partial \hat{\psi}_f}{\partial t}+\sum\left(\hat{\mu}_i^{surf}-\hat{\mu}_i^f\right)\hat{R}_i\end{aligned}\tag{138}$$

Substituting $\hat{g}_f-\hat{\psi}_f=p/\rho_f$, Eq. (138) can be finally written in Eq. (62).

REFERENCES

Abousleiman, Y., Cui, L., 1998. Poroelastic solutions in transversely isotropic media for wellbore and cylinder. International Journal of Solids and Structures 35, 4905-4929.

Anand, L., 2015. 2014 Drucker medal paper: A derivation of the theory of linear poroelasticity from chemoelasticity. Journal of Applied Mechanics 82, 111005.

Anand, L., 2017. A large deformation poroplasticity theory for microporous polymeric materials. Journal of the Mechanics and Physics of Solids 98, 126-155.

Anderson, J.L., Malone, D.M., 1974. Mechanism of osmotic flow in porous membranes. Biophysical journal 14, 957-982.

Armero, F., 1999. Formulation and finite element implementation of a multiplicative model of coupled poro-plasticity at finite strains under fully saturated conditions. Computer methods in applied mechanics and engineering 171, 205-241.

Atkin, R., Craine, R., 1976. Continuum theories of mixtures: basic theory and historical development. The Quarterly Journal of Mechanics and Applied Mathematics 29, 209-244.

Baek, S., Pence, T.J., 2009. On swelling induced degradation of fiber reinforced polymers. International Journal of Engineering Science 47, 1100-1109.

Bai, R., Yang, R.T., 2001. A thermodynamically consistent Langmuir model for mixed gas adsorption. Journal of colloid and interface science 239, 296-302.

Barbour, S., Fredlund, D., 1989. Mechanisms of osmotic flow and volume change in clay soils. Canadian Geotechnical Journal 26, 551-562.

Bedford, A., Drumheller, D.S., 1983. Theories of immiscible and structured mixtures. International Journal of Engineering Science 21, 863-960.

Bennethum, L.S., Murad, M.A., Cushman, J.H., 1997. Modified Darcy's law, Terzaghi's effective stress principle and Fick's law for swelling clay soils. Computers and Geotechnics 20, 245-266.

Biot, M.A., 1972. Theory of finite deformations of porous solids. Indiana University Mathematics Journal 21, 597-620.

Biot, M.A., 1977. Variational Lagrangian-thermodynamics of nonisothermal finite strain mechanics of porous solids and thermomolecular diffusion. International Journal of Solids and Structures 13, 579-597.
Bowen, R.M., 1980. Incompressible porous media models by use of the theory of mixtures. International Journal of Engineering Science 18, 1129-1148.
Brochard, L., Vandamme, M., Pellenq, R.-M., 2012. Poromechanics of microporous media. Journal of the Mechanics and Physics of Solids 60, 606-622.
Cheng, A.H.-D., 2016. Poroelasticity. Springer.
Chikatamarla, L., Cui, X., Bustin, R.M., 2004. Implications of volumetric swelling/shrinkage of coal in sequestration of acid gases, Coalbed Methane Symposium, Tuscaloosa, AL.
Coussy, O., 2004. Poromechanics. John Wiley & Sons, Ltd, Chichester.
Coussy, O., 2007. Revisiting the constitutive equations of unsaturated porous solids using a Lagrangian saturation concept. International Journal for Numerical and Analytical Methods in Geomechanics 31, 1675-1694.
Coussy, O., 2010. Mechanics and physics of porous solids. John Wiley & Sons.
Coussy, O., Dormieux, L., Detournay, E., 1998a. From mixture theory to Biot's approach for porous media. International Journal of Solids and Structures 35, 4619-4635.
Coussy, O., Eymard, R., Lassabatere, T., 1998b. Constitutive modeling of unsaturated drying deformable materials. Journal of Engineering Mechanics 124, 658-667.
Cui, X., Bustin, R.M., 2005. Volumetric strain associated with methane desorption and its impact on coalbed gas production from deep coal seams. Aapg Bulletin 89, 1181-1202.
Day, S., Fry, R., Sakurovs, R., 2012. Swelling of coal in carbon dioxide, methane and their mixtures. International Journal of Coal Geology 93, 40-48.
de Boer, R., 2006. Trends in continuum mechanics of porous media. Springer Science & Business Media.
de Boer, T., 1996. Highlights in the historical development of the porous media theory: toward a consistent macroscopic theory. Applied Mechanics Reviews 49, 201-262.
DeHoff, R., 2006. Thermodynamics in materials science. CRC Press.
Do, D., Nicholson, D., Do, H., 2008. Effects of adsorbent deformation on the adsorption of gases in slitlike graphitic pores: A computer simulation study. The Journal of Physical Chemistry C 112, 14075-14089.
Dolino, G., Bellet, D., Faivre, C., 1996. Adsorption strains in porous silicon. Physical Review B 54, 17919.
Duda, F.P., Souza, A.C., Fried, E., 2010. A theory for species migration in a finitely strained solid with application to polymer network swelling. Journal of the Mechanics and Physics of Solids 58, 515-529.
Eriksson, J.C., 1969. Thermodynamics of surface phase systems: V. Contribution to the thermodynamics of the solid-gas interface. Surface Science 14, 221-246.
Espinoza, D., Vandamme, M., Dangla, P., Pereira, J.M., Vidal‐Gilbert, S., 2013. A transverse isotropic model for microporous solids: Application to coal matrix adsorption and swelling. Journal of Geophysical Research: Solid Earth 118, 6113-6123.
Espinoza, D., Vandamme, M., Pereira, J.-M., Dangla, P., Vidal-Gilbert, S., 2014. Measurement and modeling of adsorptive–poromechanical properties of bituminous coal cores exposed to CO 2: Adsorption, swelling strains, swelling stresses and impact on fracture permeability. International Journal of Coal Geology 134, 80-95.
Gajo, A., 2010. A general approach to isothermal hyperelastic modelling of saturated porous media at finite strains with compressible solid constituents, Proceedings of the Royal Society of London A: Mathematical, Physical and Engineering Sciences. The Royal Society, pp. 3061-3087.
Gamson, P., Beamish, B., Johnson, D., 1996. Coal microstructure and secondary mineralization: their effect on methane recovery. Geological Society, London, Special Publications 109, 165-179.
Gamson, P.D., Beamish, B.B., Johnson, D.P., 1993. Coal microstructure and micropermeability and their effects on natural gas recovery. Fuel 72, 87-99.

George, J.S., Barakat, M., 2001. The change in effective stress associated with shrinkage from gas desorption in coal. International Journal of Coal Geology 45, 105-113.
Gor, G.Y., Bernstein, N., 2016. Revisiting Bangham's law of adsorption-induced deformation: changes of surface energy and surface stress. Physical Chemistry Chemical Physics 18, 9788-9798.
Gurtin, M.E., Fried, E., Anand, L., 2010. The mechanics and thermodynamics of continua. Cambridge University Press.
Harpalani, S., Mitra, A., 2010. Impact of CO 2 injection on flow behavior of coalbed methane reservoirs. Transport in Porous Media 82, 141-156.
Hassanizadeh, S.M., 1986. Derivation of basic equations of mass transport in porous media, Part 2. Generalized Darcy's and Fick's laws. Advances in Water Resources 9, 207-222.
Hol, S., Spiers, C.J., 2012. Competition between adsorption-induced swelling and elastic compression of coal at CO 2 pressures up to 100MPa. Journal of the Mechanics and Physics of Solids 60, 1862-1882.
Huyghe, J.M., Janssen, J., 1997. Quadriphasic mechanics of swelling incompressible porous media. International Journal of Engineering Science 35, 793-802.
Karrech, A., Poulet, T., Regenauer-Lieb, K., 2012. Poromechanics of saturated media based on the logarithmic finite strain. Mechanics of Materials 51, 118-136.
Kenyon, D.E., 1976. The theory of an incompressible solid-fluid mixture. Archive for Rational Mechanics and Analysis 62, 131-147.
Kolodner, P., Williams, H., Moe, C., 1988. Optical measurement of the Soret coefficient of ethanol/water solutions. The Journal of chemical physics 88, 6512-6524.
Kramer, D., Weissmüller, J., 2007. A note on surface stress and surface tension and their interrelation via Shuttleworth's equation and the Lippmann equation. Surface Science 601, 3042-3051.
Lapwood, E., 1948. Convection of a fluid in a porous medium, Mathematical Proceedings of the Cambridge Philosophical Society. Cambridge Univ Press, pp. 508-521.
Legros, J.C., Goemaere, P., Platten, J.K., 1985. Soret coefficient and the two-component Benard convection in the benzene-methanol system. Physical Review A 32, 1903.
Levine, J.R., 1996. Model study of the influence of matrix shrinkage on absolute permeability of coal bed reservoirs. Geological Society, London, Special Publications 109, 197-212.
Li, C., Feng, J., 2016. Adsorption-induced permeability change of porous material: a micromechanical model and its applications. Archive of Applied Mechanics 86, 465-481.
Loret, B., Rizzi, E., Zerfa, Z., 2001. Relations between drained and undrained moduli in anisotropic poroelasticity. Journal of the Mechanics and Physics of Solids 49, 2593-2619.
Nedjar, B., 2013. Formulation of a nonlinear porosity law for fully saturated porous media at finite strains. Journal of the Mechanics and Physics of Solids 61, 537-556.
Neimark, A.V., Coudert, F.o.-X., Triguero, C., Boutin, A., Fuchs, A.H., Beurroies, I., Denoyel, R., 2011. Structural transitions in MIL-53 (Cr): view from outside and inside. Langmuir 27, 4734-4741.
Ning, H., Wiegand, S., 2006. Experimental investigation of the Soret effect in acetone/water and dimethylsulfoxide/water mixtures. AIP.
Nunziato, J.W., Cowin, S.C., 1979. A nonlinear theory of elastic materials with voids. Archive for Rational Mechanics and Analysis 72, 175-201.
Nur, A., Byerlee, J.D., 1971. An exact effective stress law for elastic deformation of rock with fluids. Journal of Geophysical Research 76, 6414-6419.
Palmer, I., Mansoori, J., 1996. How permeability depends on stress and pore pressure in coalbeds: a new model, SPE Annual Technical Conference and Exhibition. Society of Petroleum Engineers.
Pan, Z., Connell, L.D., 2007. A theoretical model for gas adsorption-induced coal swelling. International Journal of Coal Geology 69, 243-252.
Pence, T.J., 2012. On the formulation of boundary value problems with the incompressible constituents constraint in finite deformation poroelasticity. Mathematical Methods in the Applied Sciences 35, 1756-1783.

Reichenauer, G., Scherer, G., 2001. Nitrogen sorption in aerogels. Journal of non-crystalline solids 285, 167-174.
Rice, J., 1978. Thermodynamics of the quasi-static growth of Griffith cracks. Journal of the Mechanics and Physics of Solids 26, 61-78.
Rice, J.R., Cleary, M.P., 1976. Some basic stress diffusion solutions for fluid - saturated elastic porous media with compressible constituents. Reviews of Geophysics 14, 227-241.
Robertson, E.P., 2005. Measurement and modeling of sorption-induced strain and permeability changes in coal. Colorado School of Mines. Arthur Lakes Library.
Rudnicki, J.W., 1986. Fluid mass sources and point forces in linear elastic diffusive solids. Mechanics of Materials 5, 383-393.
Scherer, G.W., 1986. Dilatation of porous glass. Journal of the American Ceramic Society 69, 473-480.
Selvadurai, A., Suvorov, A., 2016. Coupled hydro-mechanical effects in a poro-hyperelastic material. Journal of the Mechanics and Physics of Solids 91, 311-333.
Shen, V.K., Siderius, D.W., 2014. Elucidating the effects of adsorbent flexibility on fluid adsorption using simple models and flat-histogram sampling methods. The Journal of chemical physics 140, 244106.
Shuttleworth, R., 1950. The surface tension of solids. Proceedings of the Physical Society. Section A 63, 444.
Sorenson, S.G., Smyth, J.R., Kocirik, M., Zikanova, A., Noble, R.D., Falconer, J.L., 2008. Adsorbate-induced expansion of silicalite-1 crystals. Industrial & Engineering Chemistry Research 47, 9611-9616.
Soret, C., 1880. Sur l'etat d'équilibre que prend au point de vue de sa concentration une dissolution saline primitivement homogène dont deux parties sont portées a des températures différentes: Deuxieme note.
Svendsen, B., Hutter, K., 1995. On the thermodynamics of a mixture of isotropic materials with constraints. International Journal of Engineering Science 33, 2021-2054.
Thompson, M., Willis, J., 1991. A reformation of the equations of anisotropic poroelasticity. Journal of Applied Mechanics 58, 612-616.
Trevisan, O.V., Bejan, A., 1985. Natural convection with combined heat and mass transfer buoyancy effects in a porous medium. International Journal of Heat and Mass Transfer 28, 1597-1611.
Truesdell, C., 1962. Mechanical basis of diffusion. The Journal of Chemical Physics 37, 2336-2344.
Vandamme, M., Brochard, L., Lecampion, B., Coussy, O., 2010. Adsorption and strain: the CO 2-induced swelling of coal. Journal of the Mechanics and Physics of Solids 58, 1489-1505.
Wei, C., Muraleetharan, K.K., 2002. A continuum theory of porous media saturated by multiple immiscible fluids: I. Linear poroelasticity. International Journal of Engineering Science 40, 1807-1833.
Wijmans, J., Baker, R., 1995. The solution-diffusion model: a review. Journal of membrane science 107, 1-21.
Wilmanski, K., 1998. A thermodynamic model of compressible porous materials with the balance equation of porosity. Transport in Porous Media 32, 21-47.
Yang, R.T., 1987. Gas separation by adsorption processes. World Scientific.
Zipf, R.K., Bieniawski, Z., 1990. Mixed-mode fracture toughness testing of coal, International Journal of Rock Mechanics and Mining Sciences & Geomechanics Abstracts. Elsevier, pp. 479-493.